On physical mechanisms ~~controlling~~ enhancing air–sea CO_2 exchange

Lucía Gutiérrez-Loza[1], Erik Nilsson[1], Marcus B. Wallin[1,2], Erik Sahlée[1], and Anna Rutgersson[1]

[1]Department of Earth Sciences, Uppsala University, Uppsala, Sweden
[2]Department of Aquatic Sciences and Assessment, Swedish University of agricultural Sciences, Uppsala, Sweden

Correspondence: Lucía Gutiérrez-Loza (lucia.gutierrez_loza@geo.uu.se)

Abstract.

Reducing uncertainties in the air–sea CO_2 flux calculations is one of the major challenges when addressing the oceanic contribution in the global carbon balance. In traditional models, the air–sea CO_2 flux is estimated using expressions of the gas transfer velocity as a function of wind speed. However, other mechanisms affecting the variability in the flux at local and regional scales are still poorly understood. The uncertainties associated with the flux estimates become particularly large in heterogeneous environments such as coastal and marginal seas. Here, we investigated the air–sea CO_2 exchange at a coastal site in the central Baltic Sea using nine years of eddy covariance measurements. ~~To the best of our knowledge, this is the longest record of direct observations of CO_2 fluxes and the corresponding gas transfer velocities (k) in a marine environment.~~ Based on these observations we were able to capture the temporal variability of the air–sea CO_2 flux and other parameters relevant for the gas exchange. ~~The analysis of water-side and atmospheric control mechanisms showed that during wind speeds above 8~~Our results show that a wind-based model with similar pattern to those developed for larger basins and open sea condition can, on average, be a good approximation for k. However, in order to reduce the uncertainty associated to these averages and produce reliable short-term k estimates, additional physical processes must be considered. Using a normalized gas transfer velocity, we identified conditions associated to enhanced exchange (large k values). During high and intermediate wind speeds (above 6–8 $\mathrm{m\,s^{-1}}$~~the~~), conditions on both sides of the air–water interface were found to be relevant for the gas exchange. Our findings further suggest that at such relatively high wind speeds, sea spray ~~was~~ is an efficient mechanisms for air–sea CO_2 exchange. ~~In contrast to high wind-speed conditions, during~~ During low wind speeds (<6 $\mathrm{m\,s^{-1}}$)~~only~~, water-side ~~processes were~~ convection was found to be ~~relevant control mechanisms, in particular,~~ a relevant control mechanism. The effect of both sea spray and water-side ~~convective processes. Altogether, our results show that currently existing wind-based parametrizations of k might be good approximations as long-term averages for environments with coastal characteristics. However, in order to reduce the uncertainty associated to these averages and produce reliable short-term k estimates, additional physical processes must be considered~~convection on the gas exchange showed a clear seasonality with positive fluxes (winter conditions) being the most affected.

1 Introduction

Air–sea CO_2 exchange is an essential aspect of the global carbon cycle, having great implications for the Earth's climate. The global oceans are estimated to be net sinks of CO_2 taking up on average ca 25 % of the CO_2 emitted every year to the atmosphere due to anthropogenic activities (Friedlingstein et al., 2021). The current global ocean uptake is estimated to be between -2.0 and -3.1 $GtC\,yr^{-1}$ (Takahashi et al., 2009; Ciais et al., 2013; Friedlingstein et al., 2021). However, large uncertainties are still associated with the air–sea CO_2 flux estimates, mainly due to the incomplete understanding of the spatio-temporal variability in the controlling mechanisms. Resolving the effect of these mechanisms at the relevant temporal and spatial scales is essential to constrain the oceanic contribution in the global carbon balance.

The exchange of CO_2 across the air–sea interface can be described using the following bulk formula:

$$FCO_2 = kK_0\Delta pCO_2 = kK_0(pCO_2^w - pCO_2^a), \tag{1}$$

where the air–sea CO_2 flux (FCO_2) is a function of the gas transfer velocity (k), the difference in the partial pressure of CO_2 (ΔpCO_2) between the atmosphere and the seawater (superscripts a and w, respectively), and the salinity- and temperature-dependent solubility constant (K_0). The direction of the flux is determined by the sign of ΔpCO_2 and, by convention, positive (upward) FCO_2 represents transport from the ocean to the atmosphere (i.e. positive ΔpCO_2).

The gas transfer velocity, k, represents the efficiency of the transfer processes across the air–sea interface. For CO_2 and other slightly soluble gases, such efficiency is particularly associated to the turbulent processes occurring in the oceanic boundary layer, which ultimately control the air–sea gas exchange. The wind can be associated, directly or indirectly, with most of the turbulent process near the ocean–atmosphere interface. Thus, the traditional approach suggests that k can be represented as a function of the the wind speed since it is the largest source of kinetic energy to the upper ocean. With wind-speed data being a widely available resource globally, wind-based parametrizations of k have often been used to obtain global estimates of FCO_2 (e.g. Takahashi et al., 2009). However, large uncertainties in the estimated FCO_2 have been associated to the uncertainties in k (Woolf et al., 2019). At regional and local scales, the magnitude of these uncertainties becomes especially problematic, particularly in coastal environments where adequate representation of the physical and biogeochemical processes, and their interactions, is necessary in order to avoid large biases in the flux estimates.

In addition to the wind speed, other water-side control mechanisms are well known to play a significant role in the gas transfer processes of slightly soluble gases, such as CO_2. Furthermore, the effect of atmospheric controls, and their impact on the upper layer of the ocean, are potentially relevant (e.g. Erickson III, 1993) but seldom considered. The relative importance of these forcing mechanisms on the gas exchange is highly dependent on the characteristics near the sea surface, which in turn, can be categorized based on wind-speed regimes (e.g. Soloviev and Lukas, 2013). At moderately high wind speeds, above 8–$10\,m\,s^{-1}$, the upper layer of the ocean is generally well mixed (from the surface up to several tens of meters depth). Under these conditions, breaking waves (Zhao et al., 2003; Blomquist et al., 2017; Brumer et al., 2017), bubbles (Woolf, 1993, 1997; Bell et al., 2017), and sea spray (Andreas et al., 2016) have a significant role on air–sea interaction processes. At wind speeds lower than 4–$5\,m\,s^{-1}$, when the effects of breaking waves and wind-induced mixing are limited, convective processes in the

atmosphere (Erickson III, 1993) and the sea (Rutgersson and Smedman, 2010) become relevant. Other processes such as surface films (Pereira et al., 2018; Ribas-Ribas et al., 2018), rain (Ashton et al., 2016), Langmuir circulation (Thorpe et al., 2003), and micro-scale wave breaking (Jessup et al., 1997) might be relevant over a wider range of wind speeds, including intermediate wind velocities. In order to explain the variability and reduce the uncertainty in FCO_2 estimates, it is necessary to understand the effect of the control mechanisms on gas exchange, particularly at higher wind speeds but even relevant at low and moderate wind speeds.

Coastal oceans and marginal seas are active and heterogeneous environments in terms of both physical and biogeochemical processes. These regions have been found to be net sinks of CO_2 at global scales (Borges et al., 2005; Laruelle et al., 2010; Chen et al., 2013) with disproportionately large contributions to the global carbon system when compared to the open ocean (Laruelle et al., 2014). The complexity and heterogeneity of the coastal regions causes large spatio-temporal variability in the air–sea CO_2 exchange (Roobaert et al., 2019), variability that is rarely accounted for in global estimates.

The Baltic Sea is a semi-enclosed sea located at relatively high latitudes, stretching from 54° N to 66° N. The basin is largely affected by terrestrial inputs from surrounding watersheds and has relatively limited water exchange with the open ocean. This leads to a dynamic carbon system with significant spatio-temporal variability. A thorough assessment of the biogeochemical functioning of the Baltic Sea was recently published by Kuliński et al. (2021). In terms of the air–sea CO_2 exchange, several approaches have been used to estimate the regional fluxes, however, no consensus has been reached on the role of the Baltic Sea as a net source or sink of atmospheric CO_2 (Thomas et al., 2010; Kuliński and Pempkowiak, 2011; Norman et al., 2013b; Parard et al., 2017). In order to resolve some of the key elements associated to the air–sea CO_2 exchange, previous studies have focused on the diurnal (Honkanen et al., 2021) and seasonal (Thomas and Schneider, 1999b; Rutgersson et al., 2008; Schneider et al., 2014) variability in the partial pressure of CO_2 across the Baltic Sea, and on the spatial and temporal variability in the atmospheric CO_2 concentrations (Rutgersson et al., 2009). Furthermore, water-side convection (Rutgersson and Smedman, 2010; Norman et al., 2013b), upwelling events (Norman et al., 2013a; Jacobs et al., 2021), and ice coverage (Löffler et al., 2012) have all been recognized as important regional controls on the gas exchange. Despite these efforts, the effect of the different mechanisms modulating the air–sea gas exchange, and its variability, is still poorly understood in the Baltic Sea, as it is in many other coastal regions. Limited data availability is the main reason hindering our ability to resolve processes at relevant spatial and temporal scales. In this context, continuous and long-term monitoring of the air–sea CO_2 exchange in coastal areas is essential to improve our understanding of the gas transfer mechanisms.

In this study, we present and evaluate data collected during a nine-year period at the land-based station Östergarnsholm located on an island in the central Baltic Sea. This is, to the best of our knowledge, the longest record of air–sea CO_2 flux based on eddy covariance measurements. Using atmospheric and water-side data we evaluated different control mechanisms modulating the gas transfer velocity, k, covering a wide range of wind speed conditions.

2 Site and Data

2.1 The Östergarnsholm site

90 We used data collected between 2013 and 2021 from the Swedish marine Integrated Carbon Observation System (ICOS) station, Östergarnsholm. The station (57° 27' N, 18° 59' E) is located on a small and flat island located 4 km east of the bigger island of Gotland in the central Baltic Sea (Fig. 1). Measurements are performed in a 30 m land-based tower located on the southern tip of the island, with the base of the tower at 1.4 m above the mean sea level (Sjöblom and Smedman, 2002). The tower has been used to monitor and study the marine atmospheric boundary layer and air–sea interaction processes since 1995

95 (e.g. Smedman et al., 1999; Rutgersson et al., 2001; Högström et al., 2008; Rutgersson and Smedman, 2010; Rutgersson et al., 2020).
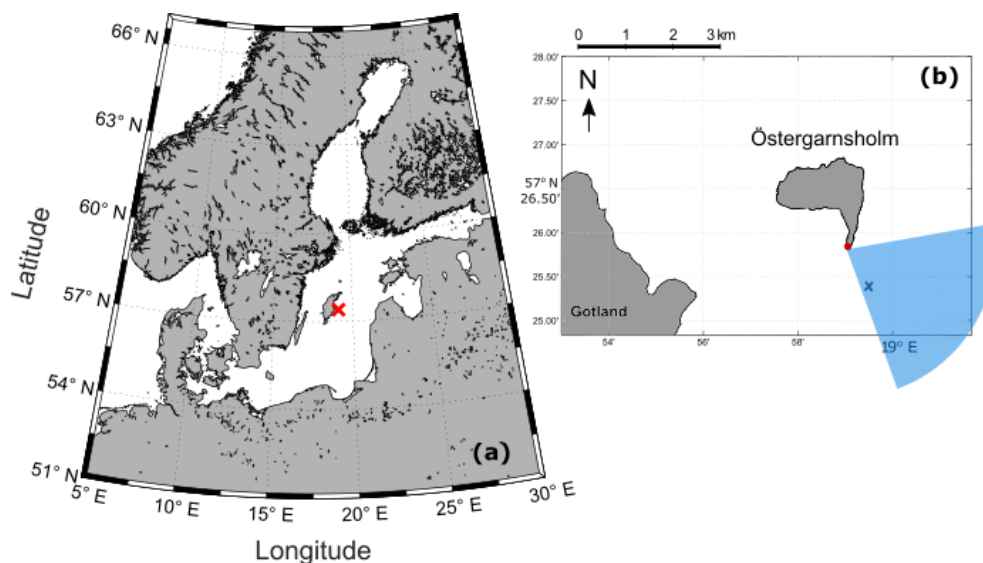
Figure 1. (a) Map of the Baltic Sea; the red cross in the central Baltic Sea indicates the location of the Östergarnsholm station. (b) Map of the Östergarnsholm station ca 4 km off from the Gotland Island; the red dot indicates the location of the tower, the blue cross is the location of the mooring with water-side instrumentation (Sect. 2.1.2), and the shaded blue area is the so-called "open-sea" sector with wind directions from $80° < WD < 160°$ (see ~~text~~ Sect. 2.1.1 for details).

2.1.1 Atmospheric data

The tower at Östergarnsholm was instrumented with high-frequency sensors for continuous turbulence measurements. Air–sea CO_2 fluxes were calculated using the fluctuations of the vertical wind component measured by a CSAT3-3D sonic anemometer

100 (Campbell Scientific, Inc., Logan, UT, USA) and the fluctuations of the atmospheric CO_2 molar densities measured with ~~a LI-7500~~ an open-path gas analyzer model LI-7500A (from 2013 to 2017) and model LI-7500RS (between 2017 and 2021) (LI-

4

COR, Inc., Lincoln, NE, USA). For details about the flux calculations see Sect. 2.2. ~~Both instruments~~ The sonic anemometer and gas analyzer were located at a height of 9 m from the tower base ~~and sampled at a~~ (i.e. 10.4 m with respect to the mean sea level), and had a sampling rate of 20 Hz. In addition to the high-frequency data, profile measurements of wind speed, wind direction, and temperature at 7, 12, 14, 20, and 29 m height were carried out at 1 Hz and averaged over 30 min periods. Relative humidity, atmospheric pressure, incoming solar radiation, and precipitation were also measured at the site.

The measurements at the Östergarnsholm site have been found to be representative of open-sea or coastal conditions depending on the wind direction (Rutgersson et al., 2020). Only data with wind directions from southeast ($80° < WD < 160°$) representing open-sea conditions were included in the analysis of the current study (Fig. 1b). For this wind sector, it was considered that no disturbances occurred in the tower measurements due to flow distortion, and that the wave field was not affected by the shallowing of the seafloor (Högström et al., 2008). Furthermore, the biogeochemical water properties and hydrographycal features were assumed to be ~~homogeneous for this sector (Rutgersson et al., 2008)~~ spatially homogeneous along this sector (Rutgersson et al., 2008, 2020), ensuring that the water-side measurements were representative of the flux footprint of the tower. A more detailed description of the Östergarnsholm site can be found in Rutgersson et al. (2020).

The flux footprint is a function used to characterize the contributions of the sources and sinks per unit area to the total flux measured at a certain point. Based on this mathematical concept, it is possible to associate the fluxes measured at a specific height with the surface exchange of any scalar (e.g. Kormann and Meixner, 2001). According to the flux footprint estimates (Kljun et al., 2015), in this study the source/sink area of the fluxes from the open-sea sector measured at 10.4 m height was located a few hundred meters upwind from the tower ~~(Fig. 2)~~. Figure 2 shows the spatial distribution of the flux contributions (in m^{-2}) for different atmospheric stability conditions. For unstable and neutral conditions, the main flux source/sink was found as a localized area near the tower. While for stable conditions, the source/sink contributions per unit area were smaller closer to the tower and rather spread over a larger region.
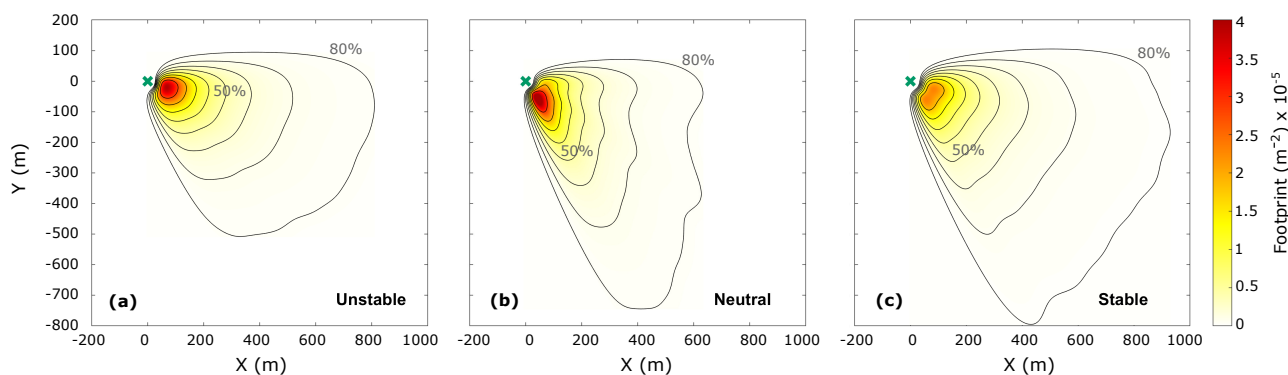
Figure 2. Average footprint distribution for (a) unstable, (b) neutral, and (c) stable atmospheric conditions. The green cross indicates the position of the tower and the contours represent the percentage of source area from 10–80 %. The flux footprint (in color) shows the spatial distribution of the contributions per unit area to the total FCO_2 (in m^{-2}). The footprint was calculated using the model developed by Kljun et al. (2015) using all data available for the open-sea sector between mid-2013 and 2020.

The atmospheric stability was represented as z/L, where z is the measurement height and L is the Monin-Obukhov length. The latter is given by $L = -u_*^3 \Theta / g \kappa \overline{w'T_s'}$, where u_* is the friction velocity, Θ is the potential temperature, $g = 9.81 \, \mathrm{m \, s^{-2}}$ is the acceleration due to gravity, $\kappa = 0.4$ is the Von Karman constant, and $\overline{w'T_s'}$ is the buoyancy flux. The sonic temperature, T_s, was considered to be almost equal to the virtual temperature, T_v, which is often used for buoyancy flux calculations (Aubinet et al., 2012). Following Sjöblom and Smedman (2002), we use $z = 10.4 \, \mathrm{m}$ as the mean measurement height with respect to the mean sea level. Here, unstable conditions were defined as $z/L \leq$ -0.05, near-neutral conditions -0.05 $< z/L <$ 0.05, and stable conditions $z/L \geq$ 0.05.

2.1.2 Water-side measurements

Water-side measurements were carried out continuously at a mooring located 1 km southeast of the tower (see Fig.1b). At the mooring, seawater temperature and partial pressure of CO_2 were measured every 30 min using a SAMI-CO_2 sensor (Sunburst Sensors, LLC, MT, USA) at a depth of 4 m. Additionally, continuous wave measurements were made with a Directional Waverider buoy located 4 km southeast of the tower (outside the domain in Fig. 1b). The Waverider buoy is operated and maintained by the Finnish Meteorological Institute (FMI). In this study, the characteristics of the sea state were represented by the significant wave height (H_s), the wave steepness calculated as H_s/L_p were L_p is the peak wavelength, and the wave age, C_p/U_{10N}, were C_p is the phase velocity of the waves and U_{10N} is the neutral equivalent wind speed at 10 m height.

Daily data of the mixed layer depth (MLD) from the Baltic Sea Reanalysis product provided by the Copernicus Marine Environment Monitoring System (CMEMS) (Von Schuckmann et al., 2016) were used as an indicator of the vertical mixing in the water column, and for the water-side convection calculations (Rutgersson and Smedman, 2010; Norman et al., 2013b). These data are freely available from CMEMS website at http://marine.copernicus.eu/services-portfolio/access-to-products/.

2.2 Data processing

High frequency data obtained at Östergarnsholm site (Sect. 2.1.1) were used for FCO_2 calculations using the eddy covariance method (Baldocchi et al., 1988; Aubinet et al., 2012) and the subsequent gas transfer velocity analysis. The turbulent fluctuations for the flux calculation (described below) were obtained following a Reynolds decomposition using an average period of 10 min. These averages were calculated as block averages from the linearly detrended time series of the 20 Hz data. The turbulent fluctuations were used to calculate variances and covariances. Other statistical moments were also calculated from the turbulent fluctuations and used as part of the quality control.

The raw wind-speed components were transformed to earth-system coordinates and corrected using a double rotation (Kaimal and Finnigan, 1994). Wind speed and direction were calculated from the corrected components to avoid effects caused by the tilting of the sonic anemometer. Following the convention, measured wind speeds were adjusted to a neutral equivalent wind speed at 10 m height (U_{10N}). Only wind directions representing open-sea conditions were used in the analysis; see Sect. 2.1.1 for details. Only periods with the three consecutive 10 min averages from $80\,° <$ WD $< 160\,°$ (i.e. open-sea sector) were included. Data with wind speeds lower than $2 \, \mathrm{m \, s^{-1}}$ ~~was excluded for~~ were excluded of the FCO_2 calculations.

155   The performance of the gas analyzer was evaluated based on the relative signal strength indicator (RSSI). Following Nilsson et al. (2018), we used the variance of the RSSI (σ^2_{RSSI}) to remove low quality data. The variance was calculated over the 10 min periods, and only data with $\sigma^2_{RSSI} < 0.001$ were considered in the analysis. Additionally, thresholds of different statistical parameters were used to ensure the homogeneity of the data and avoid outliers. Data was excluded if the absolute value of the fourth order moment of the CO_2 signal was higher than $100\,\mathrm{ppm}^4$ to filter out outliers, and the variance of the

160   vertical wind speed was $\sigma^2_w < 1e^{-6}\,\mathrm{m}^2\,\mathrm{s}^{-2}$ to exclude unrealistically low values of the vertical wind variance (low turbulence conditions).

    According to the eddy covariance method, the FCO_2 were calculated from:

$$FCO_2 = \rho_a \overline{w'c'}, \qquad\qquad (2)$$

where, ρ_a is the mean density of dry air, and the term $\overline{w'c'}$ represents the time-averaged covariance between the turbulent

165   fluctuations of the vertical wind component (w) and the dry mole fraction of the gas (c). The FCO_2 were calculated over 30 min periods by averaging three consecutive 10 min periods fulfilling all the quality-control steps. The flux was directly calculated from the CO_2 dry mole fraction (i.e. mole fraction of CO_2 relative to dry air) obtained from the measured molar densities of CO_2 relative to the ambient air. By using this direct conversion method (Sahlée et al., 2008), the corrections for dilution effects (Webb et al., 1980) were avoided. A description of the direct conversion method and detailed discussion can be

170   found in Sahlée et al. (2008). Fluxes with magnitudes below a minimum detection limit of $\pm 0.05\,\mathrm{\mu mol\,m}^{-2}\,\mathrm{s}^{-1}$ were removed. This limit was empirically defined to avoid data with low signal-to-noise ratio. In addition to FCO_2, enthalpy fluxes were also estimated from the turbulent measurements as the sum of the sensible ($\rho C_p \overline{w'T'}$) and latent ($\rho\lambda\overline{w'q'}$) heat fluxes. Furthermore, cases with high relative humidity conditions (RH$> 95\,\%$) were excluded to avoid data possibly affected by condensation on the instruments.

175   The gas transfer velocity, k, was calculated from Eq. 1 using the calculated FCO_2 (Eq. 2). The solubility constant (K_0) was determined from the relationship suggested by Weiss (1974) using a constant salinity value of 7 PSU and in situ water temperature from the SAMI sensor. Changes in the salinity, which oscillates between 6.5 and 7.5 PSU in ~~these~~ this region of the Baltic (e.g. Wesslander et al., 2010; Rutgersson et al., 2020), are not expected to have significant effects on the solubility ~~in comparison to the effect of the water temperature variability~~. The ΔpCO_2 was obtained from pCO_2^w measured with the SAMI

180   sensor, and pCO_2^a calculated from the molar densities obtained with the gas analyzer. ~~A normalized gas transfer velocity (k_{660}) was calculated as $k_{660} = k(660/Sc)^{-1/2}$, where the reference, $Sc = 660$, corresponded to the Schmidt number of CO_2 at 20 for seawater (S = 35), and Sc was the Schmidt number calculated with the corresponding in situ water temperature (T_w) for each data point.~~ Periods with $\Delta pCO_2 < \pm 50\,\mathrm{\mu atm}$ were excluded from the analysis. Furthermore, during conditions of strong water-side stratification, pCO_2^w measurements carried out at 4 m depth might not be representative of the air–sea

185   CO_2 fluxes measured at the tower. Therefore, all the data occurring during strongly stratified conditions according to the in situ observations were not considered in the analysis. Data were removed when the water-side temperature gradient (ΔT_w) was larger than $1\,^\circ\mathrm{C}$. The ΔT_w was defined as the difference between T_w measured at 4 m depth and the near-surface water

temperature (T_{ns}) measured at 0.35 m depth with the Waverider buoy. ~~Finally, scattered negative k_{660} were expected due to the stochastic behaviour of turbulence. However, more negative~~ The calculated k values were adjusted to a reference Schmidt

190 number (Sc) to compensate for temperature and salinity effects. The adjusted gas transfer velocity (k_{660}~~values than what can be explained by this inherent property of eddy covariance data were observed. There was no methodological reason to exclude such data from the data set as they fulfilled all previous quality control steps. Nonetheless, they were not used for the more detail analysis presented in Sect. 3.2.1 to Sect. 3.2.3,due to the lack of a viable physical explanation~~) was given by $k_{660} = k(660/Sc)^{-1/2}$, where $Sc = 660$ corresponds to the Schmidt number of CO_2 at $20\,^{\circ}$C for seawater (S = 35 ‰), and Sc

195 was the Schmidt number calculated with the corresponding in situ water temperature (T_w) for each data point.

The final data set, after quality control processing, consisted of 3,477 FCO_2 data points and 1,349 k_{660} data points. This amount of data corresponds to 18.7 % and 15 %, respectively, out of the total amount of data available for the open-sea sector (18,625 FCO_2 and 8,974 k_{660} data points). Further information about the rejection rates of each quality control criterion can be found in Appendix B.

200 The calculated k_{660} were used to study the effect of water-side and atmospheric control mechanisms on air–sea CO_2 exchange. ~~In order to remove the~~ A wind-speed ~~dependency from~~ relationship (k_{wind}) was calculated as the cubic (best) fit to the bin-averaged k_{660}, ~~a "residual"~~ using equidensity bins based on the wind speed percentiles, and used to obtain a normalized gas transfer velocity ~~was calculated (k_r). This residual term was calculated for each half-hourly value as the difference between~~ defined as k_{660}/k_{wind}. The use of a normalized gas transfer velocity allowed the analysis of mechanisms on k_{660}~~and the~~

205 ~~wind-based parametrization from Wanninkhof (2014) (hereafter referred to as k_{W14})~~, in addition to the effect of wind speed. For the analysis, the data were divided into three different wind-speed regimes from light breeze to moderate gale. The thresholds for these regimes were chosen depending on the expected conditions at the sea surface according to the Beaufort Scale (Barua, 2005). Low wind speeds were defined as $U_{10N} < 6\,\mathrm{m\,s^{-1}}$, covering conditions of light to moderate breeze; only ripples and small waves causing little disturbance on the surface were expected under these conditions. Intermediate conditions

210 representing moderate breezes included wind speeds of ~~$6 > U_{10N} < 8$~~ $6 \leq U_{10N} \leq 8\,\mathrm{m\,s^{-1}}$. Finally, relatively high wind-speed conditions were defined as $U_{10N} > 8\,\mathrm{m\,s^{-1}}$ when moderate to long waves were expected, whitecaps and sea spray were likely to be observed; these wind speeds correspond to fresh breeze to moderate gale.


3 Results

3.1 Oceanic and meteorological conditions: the annual cycle

215 The annual cycle, obtained using the nine years of data (2013–2021), showed a seasonal pattern in both pCO_2^w and pCO_2^a (Fig. 3a). The pCO_2^a variability was small, at least when compared to the variability in pCO_2^w. The lowest pCO_2^a were observed during the late summer and autumn with values often below 380 µatm. Higher values occurred during winter, reaching 440 µatm. While the monthly means of pCO_2^a oscillated around 410 µatm. An increasing trend in pCO_2^a was observed during the study period (not shown); a linear regression using the monthly averages suggested an increase of 0.2 ppm per month which

220 corresponds to a total increase of approximately 20 ppm during the nine-year period. Both the trend and the seasonal variability

in pCO_2^a were masked by the variability in pCO_2^w (Fig.3a). A strong seasonal pattern was observed for pCO_2^w with values higher than those in the atmosphere during the winter, and lower during summer. The seasonality in pCO_2^w in the Baltic Sea has been recognized to be strongly modulated by the biological activity (Thomas and Schneider, 1999a; Wesslander et al., 2010). Here, the lowest pCO_2^w reached values below 100 µatm during the summer of 2018. The highest values of pCO_2^w occurred

225 during the winters of 2018–2019 and 2019–2020 with observed values higher than 800 µatm. Furthermore, lower summer pCO_2^w values were observed in the last three years in comparison to previous years. In this way, the inter-annual variability of pCO_2^w was mostly noticeable in terms of an increasing amplitude of the seasonal cycle during the last years.

The monthly means of FCO_2 showed a seasonal cycle with positive fluxes during the winter and negative during the summer (Fig. 3b). This seasonal pattern in the flux was consistent with the thermodynamic forcing (i.e. $\Delta pCO_2 = pCO_2^w - pCO_2^a$)

230 which suggested an upward transport during the winter and downward during the summer. However, a high variability in the half-hourly data was observed year-round.
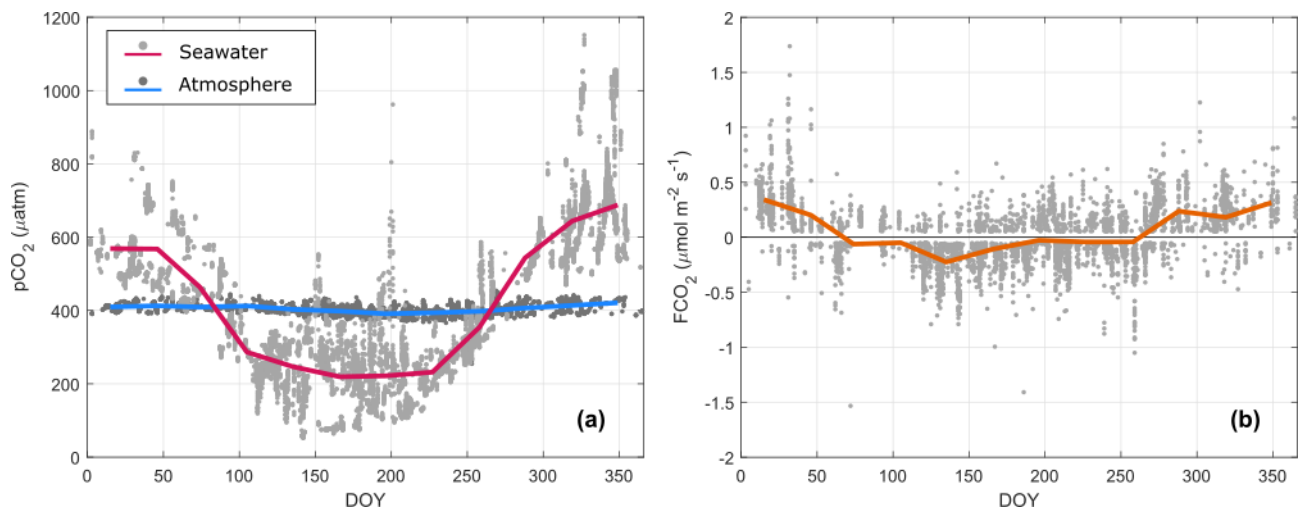
Figure 3. Annual cycle of (a) CO$_2$ partial pressure (pCO$_2$) in the seawater and in the atmosphere, and (b) air–sea CO$_2$ fluxes from eddy covariance. The dots represent the half-hourly values while the solid lines show the monthly averages.

The atmospheric and water-side variables describing the physical characteristics showed clear seasonal cycles (Fig. 4). However, a large scatter was observed from the individual half-hourly values, thus, highlighting the large variability and heterogeneity of the environment. The monthly means of wind speed and significant wave height (H_s) were higher during the autumn

235 and winter, in comparison to the summer (Fig. 4a and 4b). However, short-term events with high winds ($U_{10N} > 10\,\mathrm{m\,s^{-1}}$) and waves ($H_s \sim 3\,\mathrm{m}$) were observed during all seasons. The temperature gradient ($\Delta T = T_w - T_a$, Fig. 4c) showed that from September to February (DOY 250–50) the ocean was, on average, 1.5 °C warmer than the overlying air (i.e. positive gradient). During late spring, the atmospheric temperature was warmer than the seawater with an average ΔT of -1 °C. The enthalpy flux showed mean monthly values of 0–75 W m^{-2} (Fig. 4d). The monthly means of relative humidity (RH, Fig. 4e), ranged between

60 and 85 % throughout the year, but a large scatter was observed. Particularly during autumn and winter (DOY 250–50), when moderately low values of RH (<40 %) often occurred.
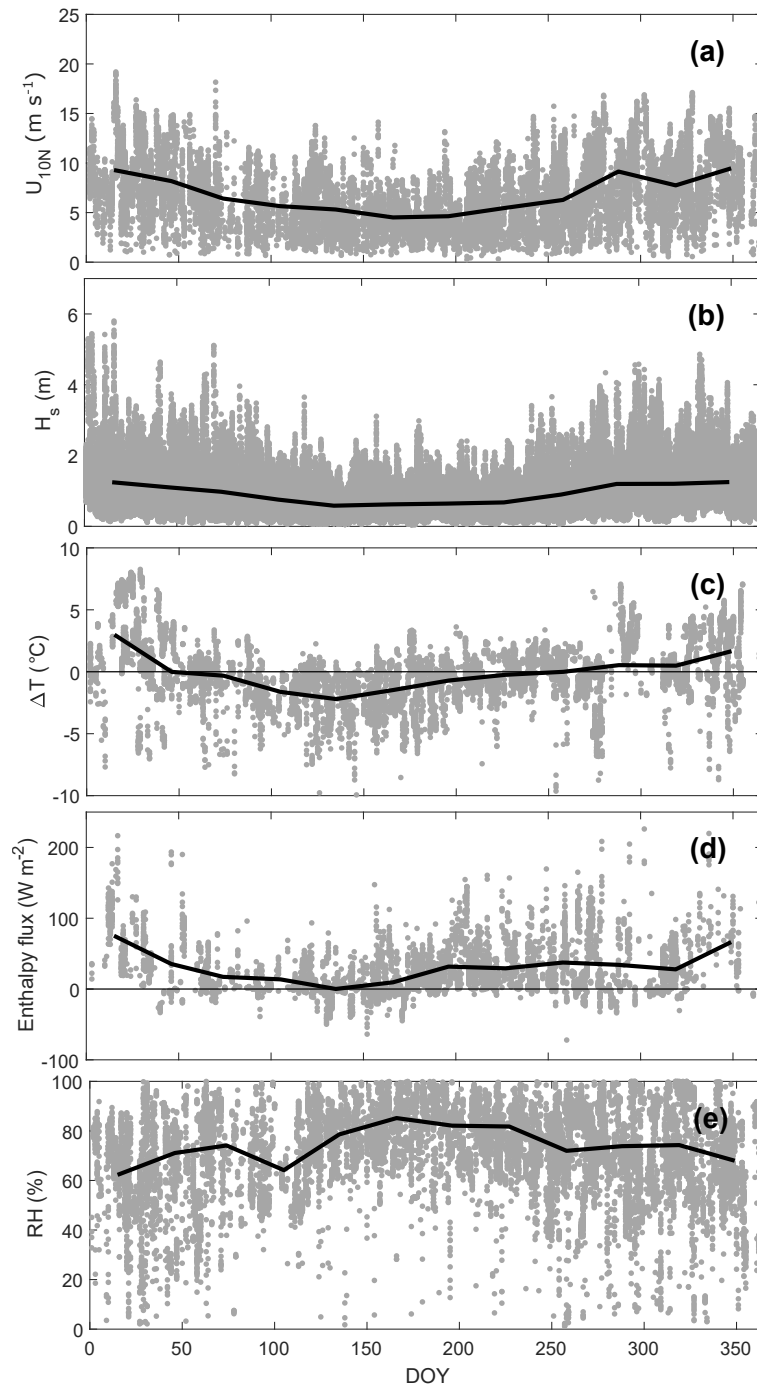
3.2 The gas transfer velocity

The gas transfer velocity, k_{660}, followed—on average—an increasing relationship with wind speed. The best fit calculated using the mean k_{660} values for each equidensity bin (130 data points) indicated a cubic relationship with wind speed, following a general agreement with other commonly-used parameterizations (Fig. 5). Even when the best fit to the bin means (k_{wind}) seemed to accurately represent the average behaviour of k_{660} as a function of wind speed ($R^2 = 0.97$), a large scatter in the k_{660} half-hourly values was observed. Only ~ 30 % of such variability in the half-hourly values was explained by a wind speed relationship (not shown).

We used the gas transfer velocity normalized by the wind-based relationship (i.e. k_{660}/k_{wind}) to evaluate the effect of individual atmospheric and water-side processes on the gas exchange. Boxplots showing the statistical summary for equidensity bins defined based on the distribution of the normalized gas transfer velocity as a function of each of the parameters were used to evaluate k_{660}/k_{wind}. Based on this analysis, we further identified the conditions inducing the strongest variability in k_{660} under different wind speed regimes (Sect. 2.2) presented in Sect. 3.2.1 to 3.2.3. The entire set of figures of k_{660}/k_{wind} can be found in Appendix A.

## 3.2.1 Controls on k_{660} at high wind speed conditions

At high wind speed conditions ($U_{10N} > 8 \, \mathrm{m \, s^{-1}}$), water-side properties such MLD and the wave field behaviour of the gas transfer velocity.

Figure 4. Annual cycle of (a) 10 m neutral wind speed, (b) significant wave height, (c) temperature gradient ($\Delta T = T_w - T_a$), (d) enthalpy flux, and (e) relative humidity. The dots are the half-hourly values while the solid black lines represent the monthly average of each parameter.
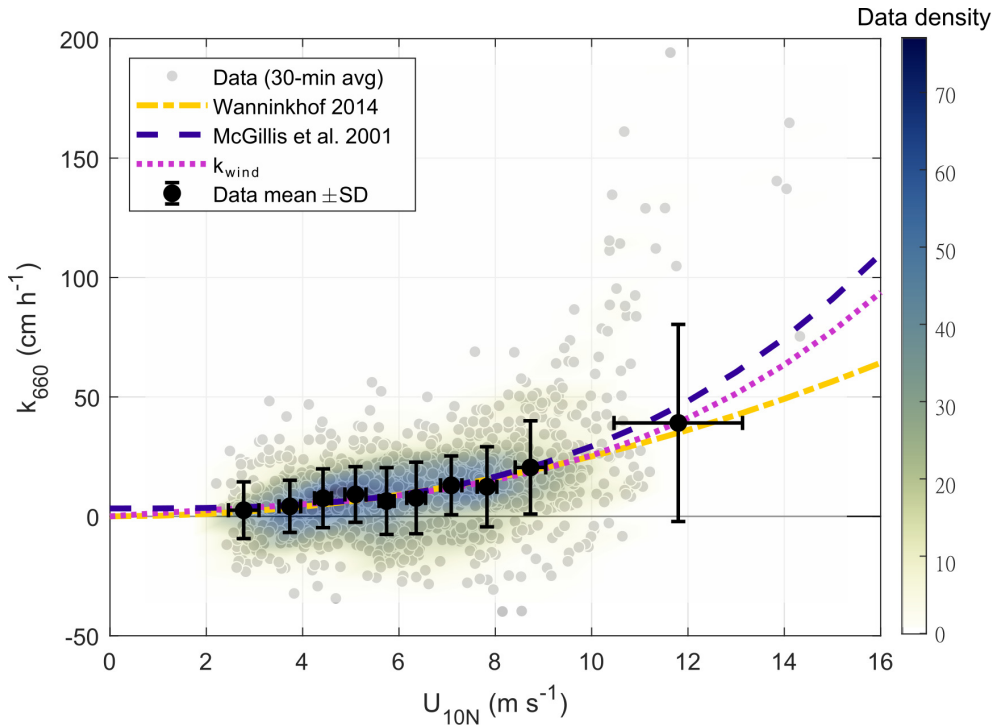
Figure 5. Gas transfer velocity for CO_2 (adjusted to a Schmidt number of 660) as a function of the 10 m neutral wind speed. The grey dots represent the half-hourly values of k_{660} for the nine-year period from 2013 to 2021. The black dots and bars, represent the k_{660} mean values and standard deviations, respectively, calculated for equi-density bins based on the wind speed percentiles; the best fit to the means is shown as the pink dotted line (k_{wind}). For reference, a quadratic (Wanninkhof, 2014) and cubic (McGillis et al., 2001) wind-based parametrizations were included. The colors in the shaded area represent the data density (in counts) with a grid bin size of $1 \, \mathrm{m \, s^{-1}}$ by $10 \, \mathrm{cm \, h^{-1}}$.
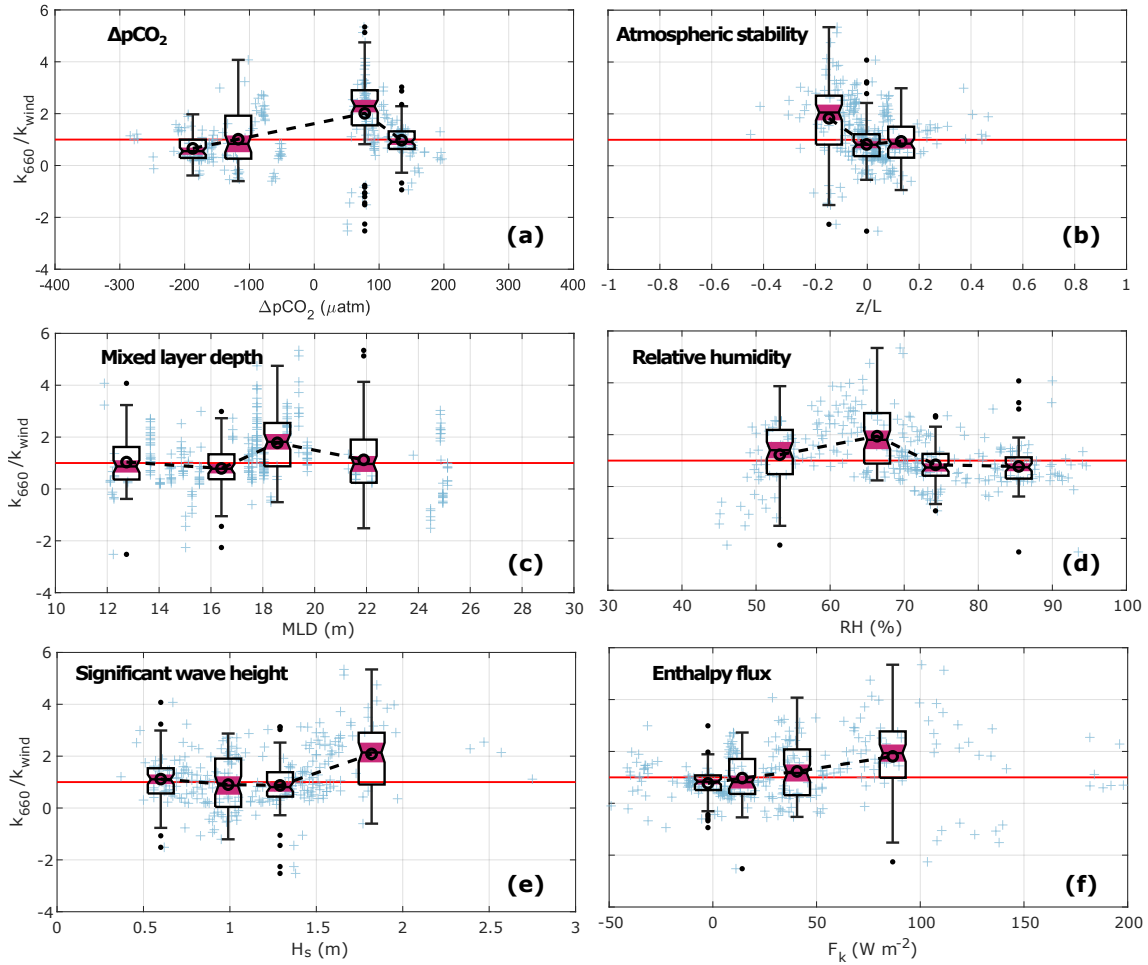
Residual gas transfer velocity ($k_r = k_{660} - k_{W14}$) as a function of the 10 neutral wind speed under high wind speed conditions. The color represents a) significant wave height, b) wave steepness (H_s/L_p), and c) wave age (C_p/U_{10N}). The vertical dashed lines mark the threshold between intermediate ($6 < U_{10N} < 8$) and high ($U_{10N} > 8$) wind speeds. The red mark in c) indicates the theoretical threshold between wind sea ($C_p/U_{10N} < 1.2$) and swell ($C_p/U_{10N} > 1.2$).

In addition to the wave field, we found . Furthermore, ΔpCO_2 and MLD to be relevant water-side parameters which were associated to the behaviour of the gas transfer velocity (Fig. ??). Note that was not only the driver of the flux defining the direction of the transport, but the characteristics of the gradient were also connected to the efficiency of the exchange. Thus, ΔpCO_2 was considered here as a water-side control due to the importance of pCO_2^w in modulating the variability of the gradient, in comparison to the rather constant values of pCO_2^a (see Sect. 3.1). Under conditions of strong gradients, where the absolute magnitude of ΔpCO_2 was higher than $200 \, \mu$atm, k_{660} followed the wind-based parametrization ($k_r \approx 0$). Nonetheless,

Particular conditions of the ~~largest values of~~ water-side parameters, were found to be linked to k_{660} ~~were not related to such strong gradients, instead, they were related to moderate positive~~ values higher than those suggested by the wind-speed

285 relationship (i.e. $k_{660}/k_{wind} > 1$), while the rest of the time, wind speed seemed to better describe the behaviour of k_{660} (i.e. $k_{660}/k_{wind} \sim 1$) (Fig. 6). Moderately positive gradients, with ΔpCO_2 ~~values in~~ of the order of 50-100 μatm, were associated with significantly higher k_{660}/k_{wind} values (Fig. ??6a). ~~Large negative values of ΔpCO_2 were, in most cases, linked to negative values of k_r, thus, lower-than-expected from~~ While under conditions of strong positive and negative gradients, k_{660} followed the wind-based ~~parametrization. While, moderate negative values of ΔpCO_2 occurred for~~ relationship; smaller gradients (both

290 positive and negative ~~k_r values. At~~) showed the largest variability. Furthermore, at these relatively high wind-speed conditions ($U_{10N} > 8 \, \mathrm{m\,s^{-1}}$), the water column was well mixed and, while some scatter is observed, the largest values of ~~k_r were associated~~ k_{660} seemed to be related with a deep mixed layer (Fig. ??b). ~~Relatively shallow MLD values remained closer to the $k_r = 0$ line and below it.~~ 6c). The combined effect of ΔpCO_2 and MLD, was strongly modulated by the seasonal patterns. During the winter, strong and persistent vertical mixing occurred along with positive ΔpCO_2 (Fig. 3a). During the

295 summer, shallower MLD and negative ΔpCO_2 were observed. Consistently, the probability distribution function showed a higher probability of positive ΔpCO_2 during the high wind speed regime (Fig. A1a) together with a wide distribution of MLD (Fig.A1b), suggesting winter conditions during a large proportion of the high wind-speed regime. On the contrary, higher probability of negative ΔpCO_2 and shallower MLD depth occurred during low wind speeds.

In addition to ΔpCO_2 and MLD, the characteristics of the wave field were—to some extent—associated to an enhanced gas

300 exchange. In particular, the highest significant wave heights ($H_s > 1.5\,\mathrm{m}$) were consistent with the largest values of k_{660}/k_{wind} (Fig. 6e). Low values of wave steepness (H_s/L_p) were observed even at the highest wind speeds with maximum values of 0.06 (Fig. A2e), much lower than the theoretical wave breaking threshold (Stokes, 1880). While the small values of the wave age, C_p/U_{10N}, (Fig. A2f) indicated growth of the wave field caused by the wind forcing over the surface. Thus, suggesting the prevalence of locally generated waves (i.e. wind sea) at these wind speed conditions.

305 Atmospheric conditions such as atmospheric stability, relative humidity, and the total enthalpy flux ~~seemed to be linked~~ were also associated to the gas exchange efficiency ~~as well (Fig. ??)~~. In terms of the atmospheric stability, ~~the differences between unstable , neutral, and stable conditions became evident at the highest wind speeds~~ a clear enhancement on k_{660} was observed during unstable conditions in comparison to k_{wind} (Fig. ??a). ~~An increased wind-speed dependency of k_{660} (and therefore of k_r) was observed under unstable conditions for wind speeds higher than 8 . While k_r remained close to zero up to~~

310 ~~10 during stable and neutral conditions. At wind speeds higher than 10~~6b). Meanwhile, during neutral and stable conditions, no significant difference was observed between k_{660} and k_{wind}. Relative humidity below 70 ~~, k_r tended to decrease with wind speed during stable conditions, and to a lesser extent under neutral conditions~~% were consistent with $k_{660}/k_{wind} > 1$, while during higher RH, the scatter in the data was low and k_{660} was well represented by k_{wind}. Furthermore, ~~high k_r values were~~ an increasing trend was observed in terms of the total enthalpy flux, with higher k_{660} values observed when high enthalpy fluxes

315 occurred~~; meanwhile, the lowest values of the enthalpy flux were associated to negative k_r values (Fig. ??b). The relative humidity seemed to also play a role, with high RH values associated to negative k_r for wind speeds higher than 10~~.

13

Figure 6. ~~Residual~~ Normalized gas transfer velocity ($k_r = k_{660} - k_{W14}k_{660}/k_{wind}$) ~~as a function of the 10 neutral wind speed~~ under high wind speed conditions ~~. The color represents~~ ($U_{10N} > 8\,\text{m s}^{-1}$) as a function of a) ~~the~~ ΔpCO_2, ~~and~~ b) ~~the~~ atmospheric stability (z/L), c) mixed layer depth (MLD), d) relative humidity (RH), e) significant wave height (H_s), and f) total enthalpy flux (F_k). The ~~vertical dashed lines mark~~ crosses represent the ~~threshold between intermediate~~ individual half-hourly values. The boxplots give a statistical summary for equidensity bins defined based on the distribution of k_{660}/k_{wind} as a function of each of the parameters (~~$6 < U_{10N} < 8$~~ see Appendix A). The median, first, and ~~high ($U_{10N} > 8$~~ third quartiles are represented in each box; the whiskers represent the minimum and maximum values, and the black dots represent the outliers; the notches highlighted in pink indicate the median's 95 ~~) wind speeds~~% confidence interval. The open circles linked with a dashed line indicate the bin means, and the horizontal red line indicates $k_{660}/k_{wind} = 1$.

Based on the analysis presented in Fig. 6, we identified a set of conditions that were associated with enhanced values of k_{660}. These conditions were characterized by positive ΔpCO_2, strong water-side mixing and dry air (RH < 70 ~~. On the contrary, low RH were observed mostly during positive k_r~~%) during unstable atmospheric stratification. A wave field with

320    $H_s > 1.5$ m, further enhanced the gas exchange. Gas transfer velocities higher than predicted, not only by k_{wind}, but also by

14

other commonly-used parametrizations were observed under these specific conditions (Fig. ??c). ~~Some low RH values linked to negative k_r were observed at wind speeds higher that 10, however, these values were also related to close-to-zero values of the enthalpy flux. According to the results~~ 7). These enhanced conditions, were observed particularly during high wind speeds, but also during the intermediate regime, and to a much lesser extent during the low wind speed conditions. When these data were excluded from the analysis, k_{660} was better represented by U_{10N} following a quadratic relationship ($R^2 = 0.62$). Furthermore, the enhanced k_{660} (blue dots in Fig. ??, ~~dry air during unstable atmospheric conditions was not only associated to large enthalpy fluxes, but it also triggered a significant increase in the efficiency of the gas exchange~~ 7), showed a wind-speed dependency of higher order (cubic) and $R^2 = 0.57$.
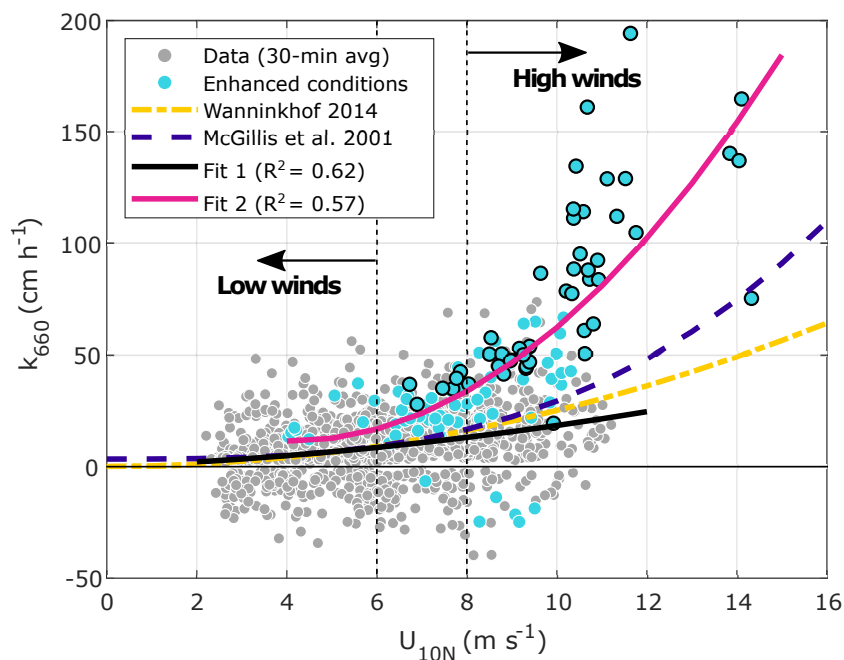
Figure 7. ~~Residual gas~~ Gas transfer velocity for CO_2 ($k_r = k_{660} - k_{W14}$ adjusted to a Schmidt number of 660) as a function of the 10 m neutral wind speed. The dots represent the half-hourly values of k_{660}. The blue dots represent k_{660} under ~~high wind speed~~ enhanced conditions (see text for details), while the blue dots with a black edge indicate cases where $H_s > 1.5$ m. The ~~color~~ black line represents ~~a~~ the best fit (quadratic) ~~atmospheric stability, b~~ to the data excluding the enhanced cases (only gray dots) ~~enthalpy flux, and c~~ while the pink line is the best fit to the enhanced data (only blue dots) ~~relative humidity~~. ~~In~~ For reference, a ~~) the filled symbols represent the bin average under each atmospheric regime~~ quadratic (Wanninkhof, 2014) and ~~the bars indicate $\pm 1\sigma$~~ cubic (McGillis et al., 2001) wind-based parametrizations were included. The wind speed regimes are separated by vertical dashed lines ~~mark the threshold between intermediate ($6 < U_{10N} < 8$) and high ($U_{10N} > 8$) wind speeds~~.

3.2.2 Controls on k_{660} under low wind-speed conditions

Under low wind-speed conditions ($U_{10N} \leq 6\,\mathrm{m\,s^{-1}}$)~~the wave field showed smaller (H_s<1) and less steep waves (Fig. ??a and b). Under these conditions, the waves tended to be older (C_p/U_{10N}>1.2, Fig. ??c), indicating a larger proportion of swell waves in comparison to the locally generated waves observed at~~, the scatter of the data was even larger than under higher wind speeds. ~~The characteristics of the wave field did not show a clear relation with the behaviour of k_r. Furthermore, the analysis of other water-side~~ Water-side parameters such as ΔpCO_2, MLD, and water-side convection helped explain part of the variability ~~in the gas transfer velocity (Fig. ??). The largest ΔpCO_2 values, with absolute magnitudes higher than 200 μatm, were observed within ±10~~ observed. Gas transfer velocities higher than predicted by k_{wind} were observed for both positive and negative gradients, showing that only under very strong negative gradients (ΔpCO_2 < -162 μatm~~of the horizontal line, i.e. $k_r \approx0$~~) the gas exchange was lower than expected by the wind-speed relationship (Fig. ~~??~~8a). ~~Positive ΔpCO_2 corresponded to positive k_r, while strong negative values of ΔpCO_2 were mostly associated with negative k_r for wind speeds below 6, but a large scatter is observed. Under these calm~~Under these calmer wind speed conditions, the values of MLD were generally low (Fig. A1b), with the lowest (MLD<15) values showing a larger scatter in k_{660} (Fig.~~??b~~A1k). The pattern of ΔpCO_2 and MLD was ~~associated~~consistent with the seasonal ~~cycles, suggesting that shallow MLD~~cycle where shallow MLD, typical of the summer months~~may~~, can hinder the downward transport of CO_2 into the sea ~~.~~(negative ΔpCO_2). The wave field showed smaller (H_s<1 m) and less steep waves. Under these conditions, the waves tended to be older (C_p/U_{10N}>1.2), indicating a larger proportion of swell waves in comparison to the locally generated waves observed at higher wind speeds. The characteristics of the wave field did not seem to induce any deviation of k_{660} with respect to k_{wind} at low wind speeds (Fig. A2).

In addition to ΔpCO_2 and the MLD, atmospheric stability and the water-side ~~convection was a relevant parameter under~~convective scale ($w*$, as defined in Jeffery et al. (2007)) were relevant parameters used to explain at least part of the variability in k_{660}. On average, lower k_{660} than expected by k_{wind} during unstable atmospheric conditions and high water-side convective scale were observed (Fig. ~~??~~8b and c). ~~Low values~~However, large variability was observed under these conditions. Meanwhile, k_{wind} seemed to better represent the behaviour of k_{660} under neutral and stable conditions, as well as during lower magnitudes of the water-side convective scale~~($w*$), as defined in Rutgersson and Smedman (2010), were observed on and below the horizontal line (i.e. $k_r \approx 0$). Meanwhile, some of the scattered data could be associated with larger values of the~~. Under low wind-speed conditions, large enthalpy fluxes were associated with k_{660}/k_{wind}<1 (Fig. 8d).

Further analysis of the data during low wind speeds and unstable atmospheric conditions showed that water-side ~~convective scale ($w* > 0.01$). Water-side convection seemed to be particularly relevant for positive fluxes, which occurred during the winter when~~convection can enhance the gas exchange. Particularly during winter, when persistent cooling of the sea surface was expected ($\Delta T > 0$), enhanced values of k_{660} were observed at low and intermediate wind speeds associated to high values of $w*$ (Fig. 9a and 10). On the contrary, low values of $w*$ were predominant during the summer months, and linked to low values of k_{660} (Fig. ~~4c)indicating cooling of the surface.~~9b and 10). Furthermore, some relatively high values of $w*$ were observed during the summer, associated to a large proportion of the negative k_{660} values observed. Under neutral and stable atmospheric
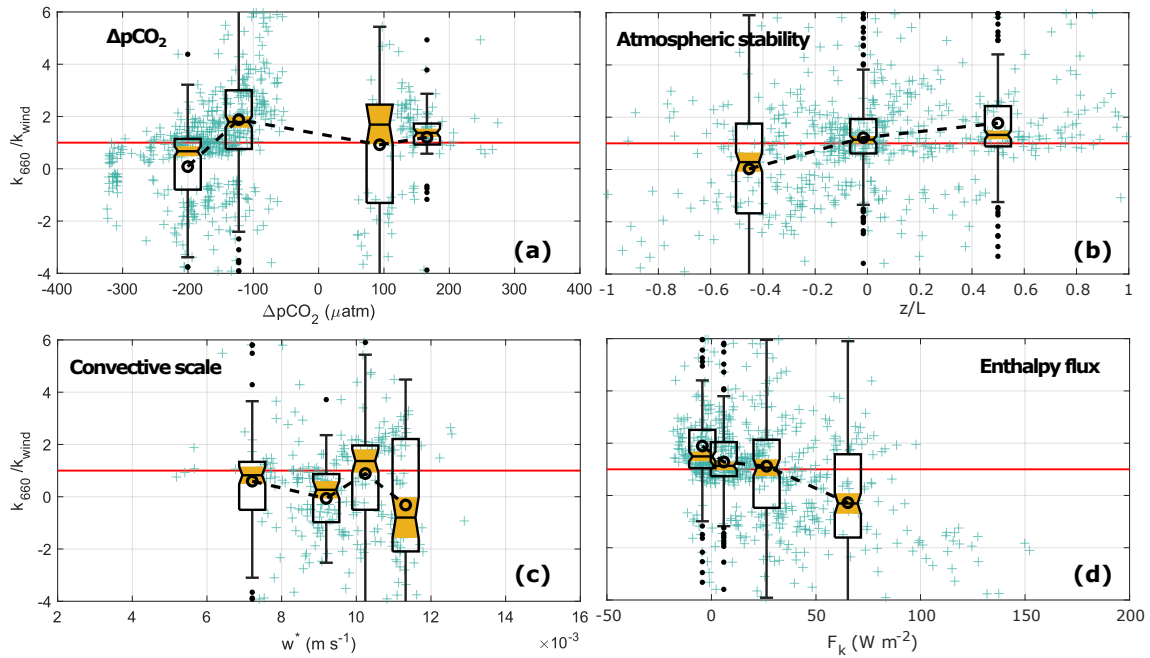
Figure 8. Normalized gas transfer velocity (k_{660}/k_{wind}) under low wind speed conditions ($U_{10N} \leq 6\,\mathrm{m\,s^{-1}}$) as a function of a) ΔpCO_2, b) atmospheric stability (z/L), c) water-side convective scale ($w*$) under unstable atmospheric conditions, and d) enthalpy flux (F_k). The crosses represent the individual half-hourly values. The boxplots give a statistical summary for equidensity bins defined based on the distribution of k_{660}/k_{wind} as a function of each of the parameters (see Appendix A). The median, first, and third quartiles are represented in each box; the whiskers represent the minimum and maximum values, and the black dots represent the outliers; the notches highlighted in yellow indicate the median's 95 % confidence interval. The open circles linked with a dashed line indicate the bin means, and the horizontal red line indicates $k_{660}/k_{wind} = 1$.

conditions, water-side convection is not a relevant mechanism (Rutgersson and Smedman, 2010; Rutgersson et al., 2011; Norman et al., 20

The rest of the scattered data which occurred during negative ΔpCO_2 and shallow MLD ~~(Fig. ??a and ??b)~~ cannot be

365   explained by water-side convection or any other parameter assessed in this study. Furthermore, the interpretation of these data should be taken with some caution as the strong stratification, relatively weak ΔpCO_2, and the possibility of strong heterogeneity in terms of the biogeochemical properties might hinder our capacity to calculate k_{660} from pCO_2^w and FCO_2. ~~Under neutral and stable atmospheric conditions, water-side convection is not a relevant mechanisms (Rutgersson and Smedman, 2010; Rutgersson et al., . At low wind speed conditions, atmospheric controls (not shown) did not play any significant role on the gas exchange.~~

370   ~~Residual gas transfer velocity ($k_r = k_{660} - k_{W14}$) as a function of the 10 neutral wind speed under low wind speed conditions. The color represents a) significant wave height, b) wave steepness (H_s/L_p), and c) wave age (C_p/U_{10N}). The vertical dashed lines mark the threshold between low ($U_{10N} < 6$) and intermediate ($6 < U_{10N} < 8$) wind speeds. The red mark in c) indicates the theoretical threshold between wind sea ($C_p/U_{10N} < 1.2$) and swell ($C_p/U_{10N} > 1.2$).~~

17
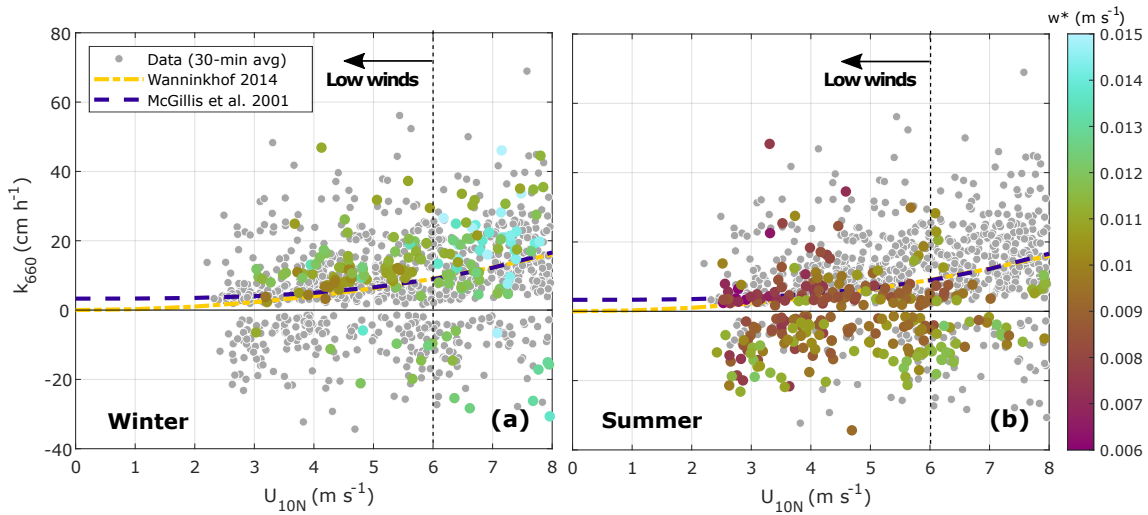
Figure 9. Gas transfer velocity for CO_2 (adjusted to a Schmidt number of 660) as a function of the 10 m neutral wind speed during a) winter and b) summer. The dots represent the half-hourly values of k_{660}. The color represents the water-side convective scale ($w*$) for data under unstable atmospheric conditions, calculated according to Rutgersson and Smedman (2010). The wind speed regimes are separated by a vertical dashed line.
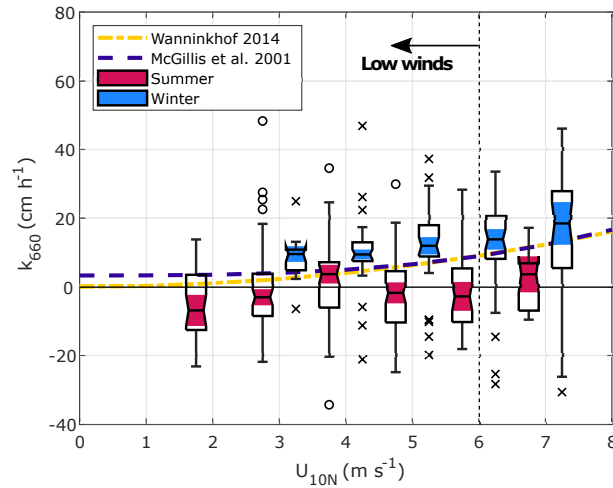
Figure 10. Boxplots of the gas transfer velocity for CO_2 (adjusted to a Schmidt number of 660) during unstable atmospheric conditions as a function of the 10 m neutral wind speed during summer (pink) and winter (blue). The median, first, and third quartiles are represented in each box; the whiskers represent the minimum and maximum values, and the circles and crosses represent the outliers; the notches highlighted in color indicate the median's 95 % confidence interval. The wind speed regimes are separated by a vertical dashed line.

Residual gas transfer velocity ($k_r = k_{660} - k_{W14}$) as a function of the 10 neutral wind speed under low wind speed conditions.
375 The color represents a) the ΔpCO_2, b) the mixed layer depth (MLD), and c) the water-side convective scale (w^*) as defined

18

3.2.3 Controls on k_{660} in the ~~transition~~ <u>intermediate wind-speed</u> range

Wind speeds between 6 and $8\,\mathrm{m\,s^{-1}}$ were considered here as the ~~transition range~~<u>between low and high wind speeds. For</u>

380 ~~convenience, the results of this transition range were included in the figures of both high and low wind speed conditions (Sect. 3.2.1 and Sect. 3.2.2, respectively). During the transition range, the atmospheric controls did not seem to be relevant (similar to low wind-speed conditions) . Furthermore, the water-side mechanisms showed a mixed behaviour.~~ <u>intermediate range. As such, the characteristics of this intermediate wind-speed range were found to be a transition in terms of the physical conditions between the low and high wind speeds (see Figures in Appendix A)</u> . The wave field showed waves with an average H_s of

385 $0.9\,\mathrm{m}$, in comparison to the 1.4 and $0.6\,\mathrm{m}$ of the high and low wind speed regimes, respectively. However, wave steepness and wave age at intermediate winds showed average values of H_s/L_p=0.03 and C_p/U_{10N}=1.1 similar to the mean values of H_s/L_p=0.03 and C_p/U_{10N}=1.0 observed at higher wind speeds. <u>However, no clear effect of the wave field was observed on k_{660} (Fig. A2g, h and i).</u> Both the wave field and the wind speed seemed to cause stronger mixing as larger values of MLD reaching the entire water column (ca $25\,\mathrm{m}$) were observed under the transition range in contrast to the more persistent

390 stratification at lower wind speeds (Fig. ~~??~~<u>A1</u>b). Values of MLD during these intermediate wind speeds were still lower, on average, than those observed during the high wind speed regime. Meanwhile, large values of w^* suggest the mixing caused by water-side convective processes during unstable atmospheric conditions might be relevant at the intermediate wind speeds~~(Fig. ??c). In terms of the thermodynamic forcing, positive values of ΔpCO_2 were associated to positive values of k_r similar to the behaviour at lower wind speeds. However, the increased mixing observed at intermediate winds seemed to also enhance fluxes~~

395 ~~during moderately positive ΔpCO_2, similar to the observed pattern during high wind speed conditions~~ <u>, in particular, during the winter</u> (Fig. ~~??~~<u>9</u>a).

4 Discussion

We used nine years of eddy-covariance-based FCO_2 data to evaluate the effect of different control mechanisms on air–sea CO_2 gas exchange. By using this long record, we were able to capture the seasonal <u>and inter-annual</u> variability of the FCO_2

400 and other parameters relevant to the gas exchange (Sect. 3.1), as well as directly assess controls on k_{660} (Sect. 3.2). <u>Direct FCO_2 measurements over long periods are necessary in other to resolve the effect of multiple parameters on the gas exchange at both short- and long-term (several years) scales.</u>

The empirically derived k_{660} values showed, ~~in general~~<u>on average</u>, a similar wind-speed dependency as ~~the~~ two wind-based parametrizations, the quadratic relationship from Wanninkhof (2014) ~~,~~<u>and</u> the cubic relationship from McGillis et al.

405 (2001) <u>(Fig. 5)</u>. These parametrizations were used as references~~and~~ <u>, and further comparison with the data presented here is beyond the scope of the study. Furthermore,</u> we considered that ~~using~~ <u>the use of</u> other commonly-used parametrizations (e.g. Wanninkhof and McGillis, 1999; Nightingale et al., 2000; Ho et al., 2006) would show similar results. ~~However~~<u>Based on the</u>

results presented here, we showed, on the one hand, that a wind-based model with a similar pattern to those developed for larger basins and open-ocean conditions, was an accurate representation ($R^2 = 0.97$) of the mean k_{660}. On the other hand, the scatter of the half-hourly data suggested that a large proportion of the short-term variability in k_{660} was not explained by variations in the wind speed(Fig. 5). Mechanisms . Previous studies have already pointed out the relevance of mechanisms other than the wind have been recognized to be relevant as controls on air–sea gas exchange processes, particularly in heterogeneous environments such as marginal and coastal seas (e.g. Upstill-Goddard, 2006; Gutiérrez-Loza et al., 2021). Based on the results presented here, we showed that wind-based parameterizations developed for larger basins and open-ocean conditions can be adequate approximations for long-term gas transfer velocity calculations, even in heterogeneous environments such as the studied areaHere, based on the analysis of atmospheric and water-side parameters, we identified conditions associated with enhanced k_{660} during high and low wind speed conditions.

We identified a set of conditions that were associated with enhanced values of k_{660} at intermediate and high wind speeds (Fig. 7). These conditions were characterized by positive ΔpCO_2 (i.e. winter conditions), unstable atmospheric stratification, strong vertical mixing in the water column (deep MLD), and low relative humidity. These conditions, affecting the upward fluxes during the winter months, resulted in an even more pronounced enhancement of k_{660} when the wave field presented high significant wave heights ($H_s > 1.5$ m). We suggest here, that the high k_{660} values observed can be potentially explained by the the effect of sea spray on air–sea CO_2 flux under the aforementioned conditions. In this hypothesis, the role of atmospheric parameters as control mechanisms is a key factor for the the otherwise water-side controlled CO_2 exchange across the sea surface. Unstable atmospheric conditions, for example, have been previously found to be associated with enhanced CO_2 transport (Andersson et al., 2019; Van Dam et al., 2021), possibly due to additional small-scale turbulence, as suggested by Andersson et al. (2019). However, we noticed conditions where the existing models failed to replicate the observations, and we further showed that in order to capture the short-term variability in k_{660} additional process need to be accounted forin this study we found that none of the individual parameters had a clear effect on k_{660}, and was rather the combination of these parameters leading to the specific conditions enhancing the exchange, potentially due to effective evaporation of droplets with relatively high pCO_2^w.

The characteristics of the wave field are one of the most important parameters involved on the air–sea gas transfer directly affecting the conditions of the interface. However, the effect of waves on gas exchange has been very seldom studied in coastal regions (e.g. Gutiérrez-Loza et al., 2018). We analyzed analysed different parameters describing the wave field (significant wave height, wave steepness, and wave age) and their effect on the gas transfer velocity. At high wind speeds, the waves were found to be locally generated by the wind (i.e. wind sea), which made it hard to separate the effect of the waves from that of the wind. The wave climate in the Baltic Sea is characterized by predominant short wind sea and scarce long swell (Soomere, 2022). Furthermore, the effect of swell waves was not relevant at high wind speed conditions, and while at lower wind speeds some effect from swell could be expected, such effect was partly excluded here as wind speeds lower than $2\,\mathrm{m\,s^{-1}}$ were removed from the analysis. Values of wave steepness suggested that there was no systematic wave breaking. However, empirical knowledge of the study site suggests the presence of breaking, particularly of the smallest/youngest waves. These

waves are not expected to generate significant bubble entrainment into the upper layer of the sea, but generation of sea spray is expected at the highest wind speeds.

The ~~effect~~ role of sea spray ~~in~~ as a control mechanisms of the air–sea gas exchange has been reported before (Andreas et al.,
445   2016, 2017). ~~However, the~~ The impact of a broken surface caused by wave breaking and ~~whitecaping~~whitecapping, has been shown to cause an asymmetric transport due to the injection of bubbles into the ocean enhancing the negative (downward) fluxes (Woolf, 1997; Leighton et al., 2018). ~~This was not seen here, instead~~However, the potential effect of such processes on positive fluxes is still unclear. Here, we found that the increase in the k_{660} was associated to the ocean-to-atmosphere (upward) transport in what we suggest is the effect of sea spray. This effect was clearly affected with the seasonal variability as the
450   increased k_{660} where observed during the winter months, when dry and cold air (colder than the ocean) are common (Fig.4c and e). During the winter months positive CO_2 gradients prevail and positive gas and heat fluxes are most often observed. High enthalpy fluxes were observed during the conditions enhancing k_{660}, however, the mechanisms through which the transport is enhanced might be different as heat and moisture are air-side controlled. Nonetheless, the increased evaporation rates most probably found during low relative humidity and unstable conditions might also play a role on CO_2 transport. Dedicated
455   analysis of the effect of bubbles and sea spray in coastal regions are still necessary. Particularly at high latitudes, where strong seasonality may cause significant differences in the forcing mechanisms modulating the influx and eflux of gas into/from the ocean (see Sect. 3.1). ~~A brief analysis of the effect of sea spray on air–sea fluxes made using a bulk algorithm for turbulent air–sea fluxes, freely available from (Andreas et al., 2008). The results showed that the large enthalpy fluxes observed under unstable conditions at high wind speeds (Fig. ??b) can be attributed to sea spray. Figure ?? shows sea spray mediated fluxes of~~
460   ~~up to 30 (up to 20 % of the total enthalpy flux) under these conditions. We suggest sea spray can enhance the transport of CO_2 across the interface, as it does with heat and moisture. Based on our results, this mechanism can be a relevant control of the gas exchange by enhancing upward CO_2 fluxes at wind speeds higher than 8–10 under unstable atmospheric conditions and low relative humidity.~~ Further data under these particular conditions is necessary to establish a better understanding of the effect of sea spray mediated gas fluxes, as it can be a relevant mechanism modulating FCO_2 at global scales.
465   ~~Residual gas transfer velocity ($k_r = k_{660} - k_{W14}$) as a function of the 10 neutral wind speed under low wind speed conditions. The color represents the sea-spray-mediated enthalpy flux calculated using a bulk algorithm for air–sea turbulent fluxes (Andreas et al., 2008).~~

Under calm wind speed conditions, with $U_{10N} < 6\,\mathrm{m\,s^{-1}}$, the effect of water-side convection was found to be relevant to explain the ~~lager~~ larger values of k_{660} during unstable atmospheric conditions at these wind speeds. Previous studies have
470   shown the effect of convective processes on the gas transfer in the Baltic Sea (Rutgersson and Smedman, 2010; Norman et al., 2013b). The same studies showed that the water-side convective processes are not relevant under stable and neutral conditions, as well as at wind speeds higher than $8\,\mathrm{m\,s^{-1}}$.

~~The ability to correctly calculate the gas transfer velocity from eddy covariance FCO_2 and ΔpCO_2 measurements is a matter of discussion. For the data presented here, this limitation was evident at low wind speeds during the summer months,~~
475   ~~when a strongly stratified and highly heterogeneous surface layer might not be well represented by the pCO_2^w measurements at 4 depth. In order to avoid this uncertainty in our k_{660} calculations, we removed data based on a ΔT_w criterion (see Sect.~~

21

2.2)Here, we found the effect of water-side convection to be strongly seasonal (Fig. 9 and 10), were a clear enhancement due to water-side convection occurred during the winter. During the summer, low values of w^* seemed to mostly follow the wind-speed relationships. However, we still observed scattered data at the lowest wind speeds corresponding to moderate ΔpCO_2 negative values and shallow MLD intermediate values of w^* can be linked with most of the negative k_{660} observed during low and intermediate wind speeds (Fig. ??a and 9b). Due to the uncertainty, we did not make further conclusions based on these data, and we encourage the reader to be cautious when interpreting these results. Thus, indicating that it was during these unstable conditions when the mismatch between the observed fluxes and ΔpCO_2 occurred. Further investigation is necessary in order to evaluate the effect of water-side convection at other temporal scales (i.e. diurnal variability), as well as the potential implications on FCO_2 at larger spatial scales.

In addition to the processes analysed in this study, there are other mechanisms which are relevant for the gas exchange in the Baltic Sea at different temporal and spatial scales. The occurrence of upwelling events can be up to 25-30% in some regions of the Baltic Sea (Lehmann et al., 2012). Norman et al. (2013a) found that the effect of these events on the annual mean FCO_2 can reach up to 25% for the Baltic Sea conditions. In this study we did not analyze the relative importance of upwelling on FCO_2 or k_{660} Upwelling is not expected to be relevant for the wind directions analyzed in this study, however, we recognize that part of the effect of upwelling in the area can be important and can have implication in the observed inter-annual variability might be caused by upwelling events. An in-depth analysis of the data is necessary to evaluate individual upwelling events captured during the nine years of measurements. Furthermore, using the parameterization parametrization suggested by Pereira et al. (2018) based on the skin temperature, we calculated a rough estimate of the effect of surfactants on our long-term k_{660}. The results suggest an overall effect of merely -0.1 %, suggesting a very small reduction of k_{660} when surfactants are taken into account. A detail analysis of the effect of surface films is beyond the scope of this study. Nevertheless, we recognize that this process might be particularly relevant in coastal seas and other shallow bodies of water. The analysis of the effect of sea ice, precipitation, Langmuir circulation, and other processes in the Baltic Sea is still pending.

We presented what we believe is the longest record of directly measured FCO_2 and the corresponding gas transfer velocities from in situ data . Eddy covariance data has been increasingly used in marine environments to study air–sea gas exchange (e.g. McGillis et al., 2001; Miller et al., 2010; Andersson et al., 2016; Gutiérrez-Loza et al., 2019). Although eddy covariance measurements have greatly contributed to the better understanding of gas exchange processes, some caveats still exist regarding this methodology. In this study, we identified two major limitations which we briefly discussed below.

First, the large amount of data that was removed from the analysis due to quality control (Sect. 2.2 and Appendix B). The criterion excluding the largest amount of data was the wind-direction selection (open-sea sector), criterion that excluded ca 85 % of the total data (Table B1). Relaxing this criterion would significantly increase the amount of data used for the k_{660} analysis. However, it would also mean including fluxes associated with more heterogeneous regions where the measured water properties might not necessarily be representative of FCO_2 (see Rutgersson et al., 2020); hence, larger uncertainties in the k_{660} estimates. Furthermore, the criterion regarding the signal quality of the gas analyser ($\sigma^2_{RSSI} <0.001$) was only fulfilled by 36.7 % of the flux data. Most of the data that was removed due to the low signal criterion occurred during precipitation events or very high wind speeds, when droplets land on the optical windows of the gas analyser. Gutiérrez-Loza et al. (2021) found that

precipitation (rain) increased the net CO_2 uptake by 4% in the Baltic Sea during 2009-2011, while Ashton et al. (2016) found that the effect of rain can lead to a 6% increase in the ocean uptake, globally. By removing the data due to low signal strength, the effects of precipitation remained unaccounted for in the analysis presented here, as well as fluxes under high wind speed conditions (above $12\text{–}14\,\mathrm{m\,s^{-1}}$), were strong mixing, bubble injection, and sea spray might be important controls on air–sea gas exchange (e.g. Blomquist et al., 2017; Bell et al., 2017). Removing small fluxes (i.e. $|FCO_2| < 0.05\,\mathrm{\mu mol\,m^{-2}\,s^{-1}}$) due to the gas analyser detection limit, might bias the net flux estimates. Therefore, we limited this study to the analysis of the half-hourly values and general seasonal patterns; however, conclusions about whether the region was an overall sink or source of CO_2 were avoided. Finally, the potential effect of swell on the CO_2 exchange at very low wind speeds was not accounted for, given that wind speeds lower than $2\,\mathrm{m\,s^{-1}}$ were removed from the analysis. The other criteria (see Table B1) were expected to cause very small biases, if any, on the data. The probability distribution of the quality controlled data set showed similar patterns compared to the initial data set (before quality control) for each parameter used in the analysis (i.e. ΔpCO_2, wind speed, wave properties, etc.). Hence, indicating that the reduced data set used for the analysis was a good representation of the conditions observed in the study area over the nine-year measurement period.

The second caveat was the large amount of negative k_{660} observed (Fig. 5). These data fulfilled every step of the quality control process, and therefore, there was no methodological reason to exclude these values from the data set. However, further investigation is needed to understand the source of these data and whether or not there is a viable physical explanation. We considered that part of the negative values observed here can be attributed to the inherent turbulent characteristics of eddy covariance measurements. Furthermore, at low wind speeds, conditions hindering k_{660} calculations (e.g. strong stratification), as well as instrumental limitations and set-up might, such as pCO_2^w measurements response time and depth, might become relevant. Furthermore, processes not accounted for such as chemical enhancement and surfactants (e.g. Ribas-Ribas et al., 2018) , might be also playing a role on the amount and distribution of negative k_{660} observed.

Regardless of the length of our data set, we still found three major limitations when addressing the effect of forcing mechanisms on air–sea gas exchange: 1) the use of a land-based station provides significant advantages, but it hinders the evaluation of the spatial variability of the exchange; 2) the intrinsic characteristics of the eddy covariance technique, in combination to the exclusion of wind directions not representative of open-sea conditions, resulted in a patchy data set with significant gaps throughout the time series; and 3) limited amount of data at high wind speeds ($U_{10N} > 10\,\mathrm{m\,s^{-1}}$) was recorded, which hindered the analysis and increases the uncertainties at those critical wind conditions. The results presented here provide significant insights on the air–sea gas exchange and its variability. Nevertheless, the limitations are still large and a continued effort from the scientific community is required.

Global coastal oceans and marginal seas are one of the most vulnerable environments subjected to the effect of climate change and anthropogenic pressures (Pachauri et al., 2014). Understanding the role of these regions in the global carbon cycle has become an essential aspect in order to address the challenges of the current and future climates. In this sense, the Baltic Sea can be seen as a test basin which provides a wide variety of physical and biogeochemical conditions. At the same time, the carbon system of the Baltic Sea has been relatively well-documented (e.g. Kuliński and Pempkowiak, 2011; Schneider and Müller, 2018), and the region has been a relevant study area in terms of mitigation and environmental management (Reusch

et al., 2018). The analysis and results presented here can be relevant for other marginal seas and coastal areas. While the potential effect of sea spray and water-side convection is certainly relevant at global scales, and further investigation is encouraged.

5 Conclusions

We presented a large data set of directly measured air–sea CO_2 fluxes by eddy covariance from a land-based station in the Baltic Sea. The forcing mechanisms acting on the surface of the ocean and their relative effect on the gas exchange can widely vary depending on the wind-speed. Therefore, the air–sea gas exchange, controlled by such forcing mechanisms, can also be expected to be affected in different ways depending on the wind-speed regime. We investigated the effect of the water-side and atmospheric conditions on the gas transfer velocity under relatively high, intermediate, and low wind speed regimes.

At high wind speeds $(U_{10N} > 8\,\mathrm{m\,s^{-1}})$, large k_{660} values were observed in what we identified to be cold and dry air, under unstable atmospheric conditions. We suggest, based on these results, that sea spray might be one of the most effective mechanisms enhancing air–sea CO_2 fluxes under these conditions, partly due to large evaporation rates. The effect of the wave field was particularly evident in terms of the significant wave height, with high gas transfer velocity values occurring when large values of H_s were observed. However, the effect of the wave field was not completely decoupled from the effect of the wind given that most of the waves were locally generated. Under low wind speed conditions $(U_{10N} < 6\,\mathrm{m\,s^{-1}})$, water-side convection was the only parameter explaining part of the variability on k_r, particularly during the winter. Intermediate wind speeds showed a mixed behaviour, thus, we defined these wind speeds as a transition range. Under these intermediate wind speed conditions, the effect of sea spray is still relevant, similar to the behaviour at higher winds. While convective processes enhanced k_{660} during winter, as it does at lower wind speeds.

A wind-based model, showing a similar pattern as currently existing wind-based parametrizations, showed to adequately represent the average behaviour of k_{660}. However, further investigation of parameters affecting the seasonal and inter-annual variability of the fluxes is needed to improve our understanding of air–sea gas exchange and adequately represent k_{660} at shorter time scales. Similarly, a detailed analysis of bubble- and sea-spray-mediated fluxes is needed to contribute to the understanding of CO_2 fluxes in the coastal regions, and other heterogeneous environments where the asymmetric behaviour of the transport might have strong implications.

Appendix A: Normalized gas transfer velocity

580 The full set of figures showing the normalized gas transfer velocity (k_{660}/k_{wind}) vs each of the parameters analysed in this study, are presented here. The parameters are divided in water-side control mechanisms (Fig. A1), wave field characteristics (Fig. A2), and atmospheric control mechanisms (Fig. A3). Each figure also include the probability distribution function (PDF) of each variable for high, intermediate, and low wind speeds to highlight the difference between the wind regimes.
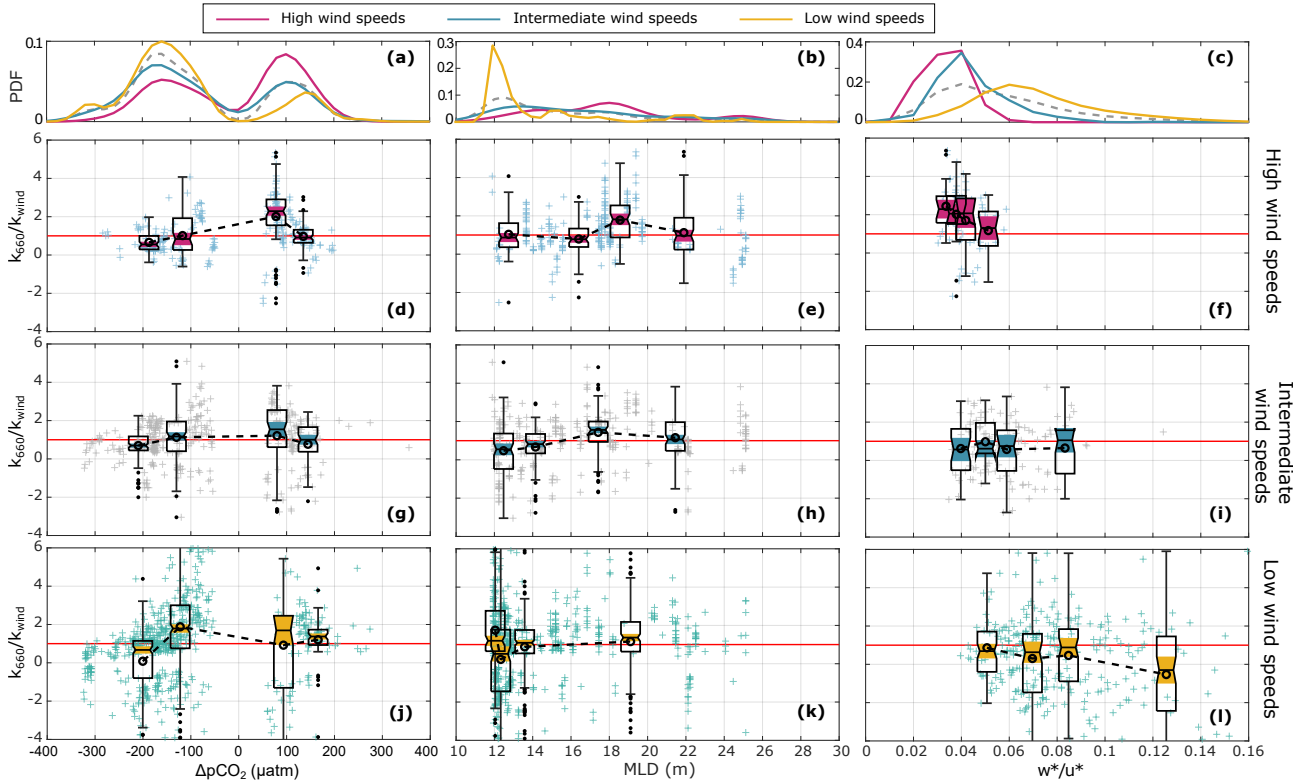
Figure A1. Water-side control mechanisms: ΔpCO_2 (left), mixed layer depth (center), and water-side convective scale normalized with the friction velocity ($w*/u*$) (right). Top panels a),b), and c) show the probability distribution function (PDF). Panels d) to l) show the normalized gas transfer velocity (k_{660}/k_{wind}) under high (upper), intermediate (middle) and low wind speeds (lower). The crosses represent the individual half-hourly values. The boxplots give a statistical summary for equidensity bins defined based on the distribution of k_{660}/k_{wind} as a function of each of the parameters. The median, first, and third quartiles are represented in each box; the whiskers represent the minimum and maximum values, and the black dots represent the outliers; the notches highlighted in yellow indicate the median's 95 % confidence interval. The open circles linked with a dashed line indicate the bin means, and the horizontal red line indicates $k_{660}/k_{wind} = 1$.
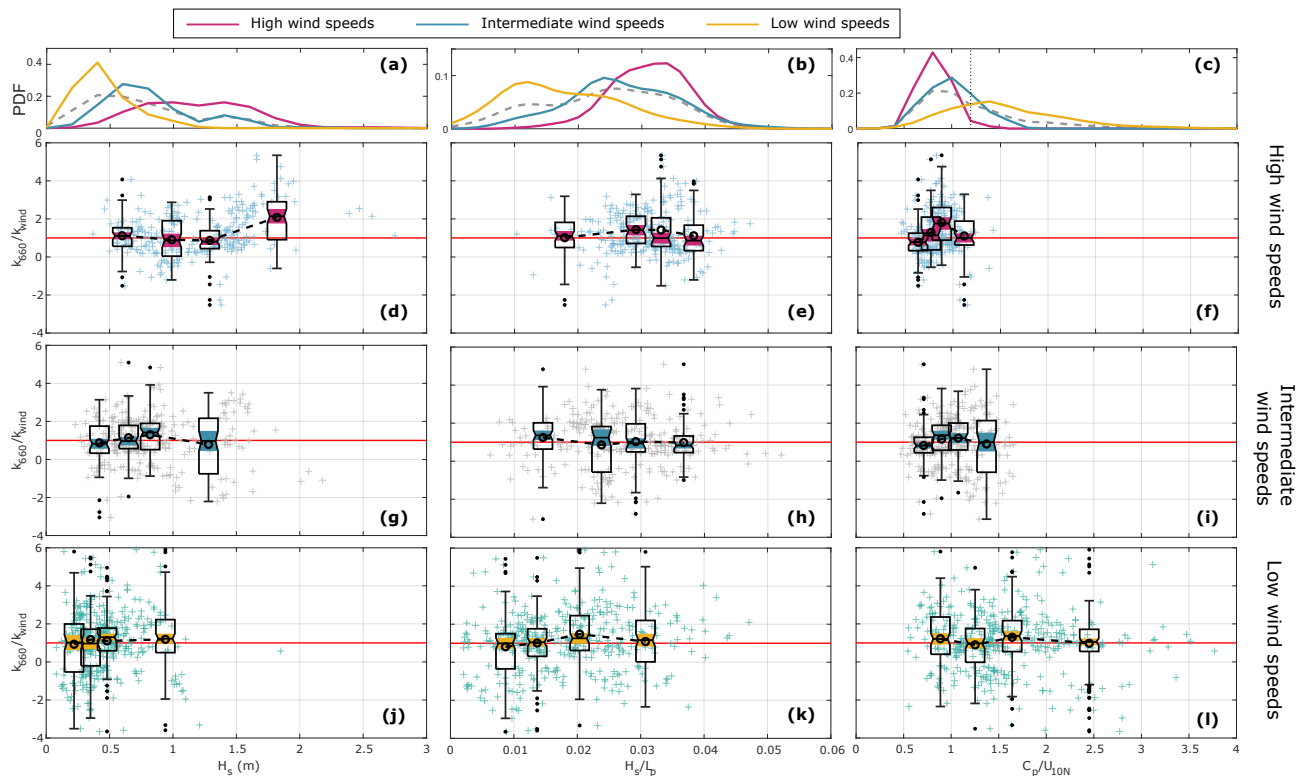
Figure A2. Same as in Fig. A1 for wave-field characteristics: significant wave height (left), wave steepness (center), and wave age (right).

Appendix B: Quality control statistics

During the nine-year record between 2013 and 2021, we recorded 125,001 FCO_2 data points and 66,475 k_{660} data points out of the maximum possible of 157,776 (half hours in nine years). However, strict quality control and post-processing analysis was necessary to ensure that only high-quality data was used for the flux calculations using the eddy covariance method (See Sect. 2.2). A significant amount of data was removed from the data set based on these criteria. Information about the relative importance of each criterion of the quality control is presented in Table B1.

The wind direction selection criterion (i.e. using only the open-sea sector) is the procedure that rejects the largest amount of data from the data set (Table B1). Considering that the total amount of data for this sector, before the quality control, was 18,625 FCO_2 and 8,974 k_{660} data points. Thus, the final data set consisted of 18.7 % and 15.0 % of the open-sea initial data for FCO_2 and k_{660}, respectively; This corresponded to 3,477 and 1,349 data points, respectively.

The wind direction selection (i.e. using only the open-sea sector) is the procedure that rejects the largest amount of data from the data set (Table B1). Considering that the total amount of data for this sector was 18,625 FCO_2 and 8,974 k_{660} data points before quality control, the final data set consisted of 18.7 % and 15.0 % of the open-sea initial data for FCO_2 and k_{660}, respectively. This corresponded to 3,477 FCO_2 and 1,349 k_{660} data points.
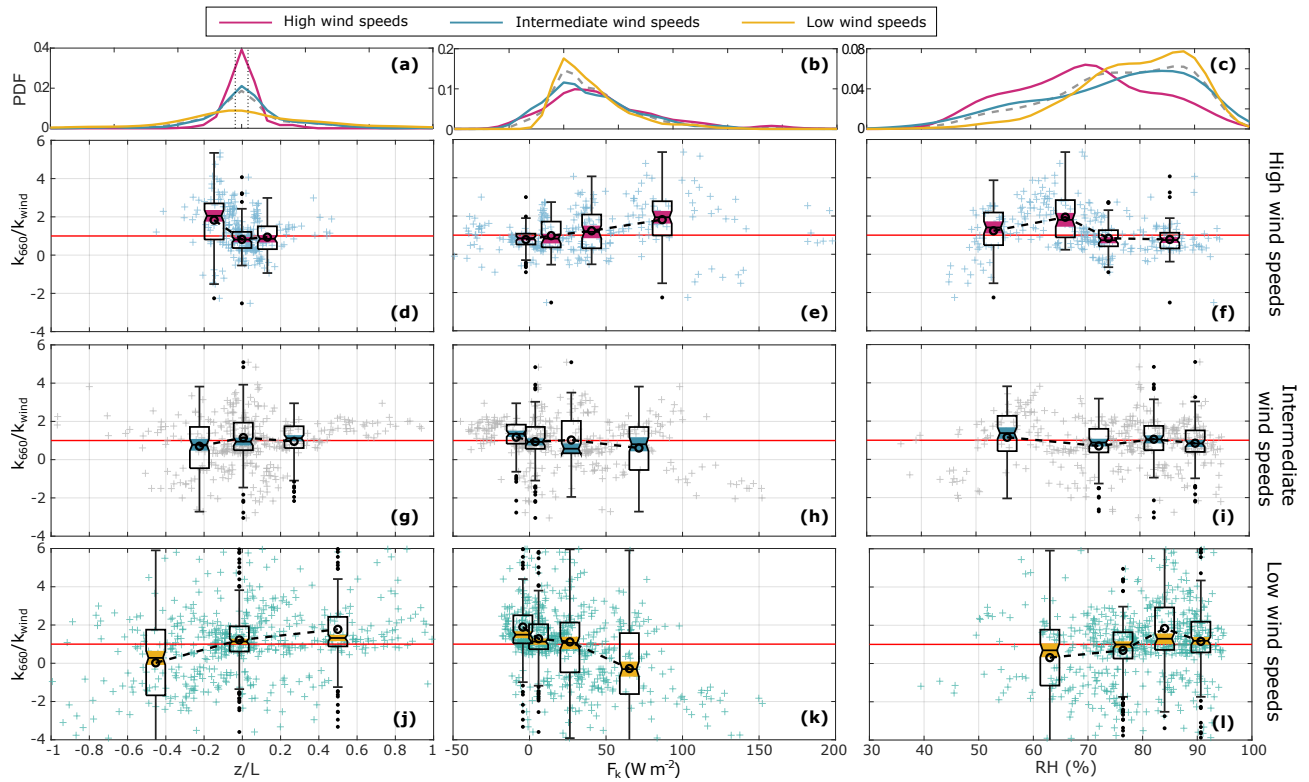
Figure A3. Same as in Fig. A1 for atmospheric control mechanisms: atmospheric stability (left), total enthalpy flux (center), and relative humidity (right)

Table B1. Percentage of data that successfully fulfill each individual quality control criterion. The percentages are relative to the total recorded amount of data (100% = 125,001 for FCO_2 and 100% = 66,475 for k_{660}).

Quality control criteria	FCO_2 data (%)	k_{660} data (%)
$U_{min} = 2\,\mathrm{m\,s^{-1}}$	95.1	94.5
Signal quality ($\sigma^2_{RSSI} < 0.001$)	36.7	41.7
Turbulence level ($\sigma^2_w > 1e^{-6}\,\mathrm{m^2\,s^{-2}}$)	99.4	99.4
Remove outliers	80.0	81.7
$|FCO_2|_{min} = 0.05\,\mathrm{\mu mol\,m^{-2}\,s^{-1}}$	51.4	48.4
$|\Delta pCO_2|_{min} = 50\,\mathrm{\mu atm}$	N/A	41.3
RH < 95 %	89.2	90.3
Open-sea sector ($80° < WD < 160°$)	14.9	13.5
$|\Delta T_w|_{max} = 1\,°\mathrm{C}$	N/A	77.6

N/A = Not applicable. The corresponding criterion has no impact on the resulting amount of data.

References

Andersson, A., Rutgersson, A., and Sahlée, E.: Using eddy covariance to estimate air–sea gas transfer velocity for oxygen, Journal of Marine Systems, 159, 67–75, 2016.

Andersson, A., Sjöblom, A., Sahlée, E., Falck, E., and Rutgersson, A.: Enhanced air–sea exchange of heat and carbon dioxide over a high Arctic Fjord during unstable very-close-to-neutral conditions, Boundary-Layer Meteorology, 170, 471–488, 2019.

Andreas, E., Vlahos, P., and Monahan, E.: The potential role of sea spray droplets in facilitating air-sea gas transfer, in: IOP conference series: earth and environmental science, vol. 35, p. 012003, IOP Publishing, 2016.

Andreas, E. L., Persson, P. O. G., and Hare, J. E.: A bulk turbulent air–sea flux algorithm for high-wind, spray conditions, Journal of Physical Oceanography, 38, 1581–1596, 2008.

Andreas, E. L., Vlahos, P., and Monahan, E. C.: Spray-mediated air-sea gas exchange: the governing time scales, Journal of Marine Science and Engineering, 5, 60, 2017.

Ashton, I. G., Shutler, J. D., Land, P. E., Woolf, D. K., and Quartly, G. D.: A sensitivity analysis of the impact of rain on regional and global sea–air fluxes of CO_2, PloS one, 11, 2016.

Aubinet, M., Vesala, T., and Papale, D.: Eddy covariance: a practical guide to measurement and data analysis, Springer Science & Business Media, 2012.

Baldocchi, D. D., Hincks, B. B., and Meyers, T. P.: Measuring biosphere–atmosphere exchanges of biologically related gases with micrometeorological methods, Ecology, 69, 1331–1340, 1988.

Barua, D. K.: Beaufort wind scale, Encyclopedia of Coastal Science. Dordrecht: Springer Netherlands, 2005.

Bell, T. G., Landwehr, S., Miller, S. D., De Bruyn, W. J., Callaghan, A. H., Scanlon, B., Ward, B., Yang, M., and Saltzman, E. S.: Estimation of bubble-mediated air–sea gas exchange from concurrent DMS and CO_2 transfer velocities at intermediate–high wind speeds, Atmospheric Chemistry and Physics, 17, 9019–9033, 2017.

Blomquist, B., Brumer, S., Fairall, C., Huebert, B., Zappa, C., Brooks, I., Yang, M., Bariteau, L., Prytherch, J., Hare, J., et al.: Wind speed and sea state dependencies of air–sea gas transfer: Results from the High Wind speed Gas exchange Study (HiWinGS), Journal of Geophysical Research: Oceans, 122, 8034–8062, 2017.

630 Borges, A. V., Delille, B., and Frankignoulle, M.: Budgeting sinks and sources of CO_2 in the coastal ocean: Diversity of ecosystems count, Geophysical Research Letters, 32, L14 601, 2005.

Brumer, S. E., Zappa, C. J., Blomquist, B. W., Fairall, C. W., Cifuentes-Lorenzen, A., Edson, J. B., Brooks, I. M., and Huebert, B. J.: Wave-related Reynolds number parameterizations of CO_2 and DMS transfer velocities, Geophysical Research Letters, 44, 9865–9875, 2017.

635 Chen, C.-T. A., Huang, T.-H., Chen, Y.-C., Bai, Y., He, X., and Kang, Y.: Air–sea exchanges of CO_2 in the world's coastal seas, Biogeosciences, 10, 2013.

Ciais, P., Sabine, C., Bala, G., Bopp, L., Brovkin, V., Canadell, J., Chhabra, A., DeFries, R., Galloway, J., Heimann, M., et al.: Carbon and other biogeochemical cycles, in: Climate change 2013: the physical science basis. Contribution of Working Group I to the Fifth Assessment Report of the Intergovernmental Panel on Climate Change, edited by Stocker, T., Qin, D., Plattner, G.-K., Tignor, M., Allen, 640 S., Boschung, J., Nauels, A., Xia, Y., Bex, V., and Midgley, P., pp. 465–570, Cambridge University Press, 2013.

Erickson III, D. J.: A stability dependent theory for air-sea gas exchange, Journal of Geophysical Research: Oceans, 98, 8471–8488, 1993.

Friedlingstein, P., Jones, M. W., O'Sullivan, M., Andrew, R. M., Bakker, D. C. E., Hauck, J., Le Quéré, C., Peters, G. P., Peters, W., Pongratz, J., et al.: Global Carbon Budget 2021, Earth System Science Data Discussions, 2021, 1–191, https://doi.org/10.5194/essd-2021-386, 2021.

Gutiérrez-Loza, L., Ocampo-Torres, F. J., and García-Nava, H.: The Effect of Breaking Waves on CO_2 Air–Sea Fluxes in the Coastal Zone, 645 Boundary-Layer Meteorology, 168, 343–360, 2018.

Gutiérrez-Loza, L., Wallin, M. B., Sahlée, E., Nilsson, E., Bange, H. W., Kock, A., and Rutgersson, A.: Measurement of air-sea methane fluxes in the Baltic Sea using the eddy covariance method, Frontiers in Earth Science, 7, 93, 2019.

Gutiérrez-Loza, L., Wallin, M. B., Sahlée, E., Holding, T., Shutler, J. D., Rehder, G., and Rutgersson, A.: Air–sea CO2 exchange in the Baltic Sea—A sensitivity analysis of the gas transfer velocity, Journal of Marine Systems, 222, 103 603, 2021.

650 Ho, D. T., Law, C. S., Smith, M. J., Schlosser, P., Harvey, M., and Hill, P.: Measurements of air–sea gas exchange at high wind speeds in the Southern Ocean: Implications for global parameterizations, Geophysical Research Letters, 33, 2006.

Högström, U., Sahlée, E., Drennan, W. M., Kahma, K. K., Smedman, A.-S., Johansson, C., Pettersson, H., Rutgersson, A., Tuomi, L., Zhang, F., and Johansson, M.: Momentum fluxes and wind gradients in the marine boundary layer: A multi platform study, Boreal environment research, 13, 475–502, 2008.

655 Honkanen, M., Müller, J. D., Seppälä, J., Rehder, G., Kielosto, S., Ylöstalo, P., Mäkelä, T., Hatakka, J., and Laakso, L.: The diurnal cycle of pCO$_2$ in the coastal region of the Baltic Sea, Ocean Science, 17, 1657–1675, 2021.

Jacobs, E., Bittig, H. C., Gräwe, U., Graves, C. A., Glockzin, M., Müller, J. D., Schneider, B., and Rehder, G.: Upwelling-induced trace gas dynamics in the Baltic Sea inferred from 8 years of autonomous measurements on a ship of opportunity, Biogeosciences, 18, 2679–2709, 2021.

660 Jeffery, C., Woolf, D., Robinson, I., and Donlon, C.: One-dimensional modelling of convective CO_2 exchange in the Tropical Atlantic, Ocean Modelling, 19, 161–182, 2007.

Jessup, A., Zappa, C. J., and Yeh, H.: Defining and quantifying microscale wave breaking with infrared imagery, Journal of Geophysical Research: Oceans, 102, 23 145–23 153, 1997.

Kaimal, J. C. and Finnigan, J. J.: Atmospheric boundary layer flows: their structure and measurement, Oxford university press, 1994.

665   Kljun, N., Calanca, P., Rotach, M., and Schmid, H. P.: A simple two-dimensional parameterisation for Flux Footprint Prediction (FFP), Geoscientific Model Development, 8, 3695–3713, 2015.

Kormann, R. and Meixner, F. X.: An analytical footprint model for non-neutral stratification, Boundary-Layer Meteorology, 99, 207–224, 2001.

Kuliński, K. and Pempkowiak, J.: The carbon budget of the Baltic Sea, Biogeosciences, 8, 3219–3230, 2011.

670   Kuliński, K., Rehder, G., Asmala, E., Bartosova, A., Carstensen, J., Gustafsson, B., Hall, P. O., Humborg, C., Jilbert, T., Jürgens, K., et al.: Baltic earth assessment report on the biogeochemistry of the Baltic Sea, Earth System Dynamics Discussions, 2021, 1–93, 2021.

Laruelle, G. G., Dürr, H. H., Slomp, C. P., and Borges, A. V.: Evaluation of sinks and sources of CO_2 in the global coastal ocean using a spatially-explicit typology of estuaries and continental shelves, Geophysical Research Letters, 37, 2010.

Laruelle, G. G., Lauerwald, R., Pfeil, B., and Regnier, P.: Regionalized global budget of the CO_2 exchange at the air-water interface in
675   continental shelf seas, Global biogeochemical cycles, 28, 1199–1214, 2014.

Lehmann, A., Myrberg, K., and Höflich, K.: A statistical approach to coastal upwelling in the Baltic Sea based on the analysis of satellite data for 1990–2009, Oceanologia, 54, 369–393, 2012.

Leighton, T. G., Coles, D. G., Srokosz, M., White, P. R., and Woolf, D. K.: Asymmetric transfer of CO_2 across a broken sea surface, Scientific reports, 8, 1–9, 2018.

680   Löffler, A., Schneider, B., Perttilä, M., and Rehder, G.: Air–sea CO_2 exchange in the Gulf of Bothnia, Baltic Sea, Continental Shelf Research, 37, 46–56, 2012.

McGillis, W. R., Edson, J. B., Hare, J. E., and Fairall, C. W.: Direct covariance air–sea CO_2 fluxes, J. Geophys. Res.-Oceans, 106, 16 729–16 745, 2001.

Miller, S. D., Marandino, C., and Saltzman, E. S.: Ship-based measurement of air-sea CO2 exchange by eddy covariance, Journal of Geo-
685   physical Research: Atmospheres, 115, 2010.

Nightingale, P. D., Malin, G., Law, C. S., Watson, A. J., Liss, P. S., Liddicoat, M. I., Boutin, J., and Upstill-Goddard, R. C.: In situ evaluation of air–sea gas exchange parameterizations using novel conservative and volatile tracers, Global Biogeochemical Cycles, 14, 373–387, 2000.

Nilsson, E., Bergström, H., Rutgersson, A., Podgrajsek, E., Wallin, M. B., Bergström, G., Dellwik, E., Landwehr, S., and Ward, B.: Evaluating
690   humidity and sea salt disturbances on CO_2 flux measurements, Journal of Atmospheric and Oceanic Technology, 35, 859–875, 2018.

Norman, M., Parampil, S. R., Rutgersson, A., and Sahlée, E.: Influence of coastal upwelling on the air–sea gas exchange of CO_2 in a Baltic Sea Basin, Tellus B: Chemical and Physical Meteorology, 65, 21 831, 2013a.

Norman, M., Rutgersson, A., and Sahlée, E.: Impact of improved air–sea gas transfer velocity on fluxes and water chemistry in a Baltic Sea model, Journal of Marine Systems, 111, 175–188, 2013b.

695   Pachauri, R. K., Allen, M. R., Barros, V. R., Broome, J., Cramer, W., Christ, R., Church, J. A., Clarke, L., Dahe, Q., Dasgupta, P., et al.: Climate change 2014: synthesis report. Contribution of Working Groups I, II and III to the fifth assessment report of the Intergovernmental Panel on Climate Change, Ipcc, 2014.

Parard, G., Rutgersson, A., Parampil, S. R., and Charantonis, A. A.: The potential of using remote sensing data to estimate air–sea CO_2 exchange in the Baltic Sea, Earth System Dynamics, 8, 1093–1106, 2017.

700   Pereira, R., Ashton, I., Sabbaghzadeh, B., Shutler, J. D., and Upstill-Goddard, R. C.: Reduced air–sea CO2 exchange in the Atlantic Ocean due to biological surfactants, Nature Geoscience, 11, 492–496, 2018.

Reusch, T. B., Dierking, J., Andersson, H. C., Bonsdorff, E., Carstensen, J., Casini, M., Czajkowski, M., Hasler, B., Hinsby, K., Hyytiäinen, K., et al.: The Baltic Sea as a time machine for the future coastal ocean, Science Advances, 4, 2018.

Ribas-Ribas, M., Helleis, F., Rahlff, J., and Wurl, O.: Air–Sea CO_2 exchange in a large annular wind-wave tank and the effects of surfactants, Frontiers in Marine Science, p. 457, 2018.

Roobaert, A., Laruelle, G. G., Landschützer, P., Gruber, N., Chou, L., and Regnier, P.: The Spatiotemporal Dynamics of the Sources and Sinks of CO_2 in the Global Coastal Ocean, Global Biogeochemical Cycles, 33, 1693–1714, https://doi.org/https://doi.org/10.1029/2019GB006239, 2019.

Rutgersson, A. and Smedman, A. S.: Enhanced air–sea CO_2 transfer due to water-side convection, Journal of Marine systems, 80, 125–134, 2010.

Rutgersson, A., Smedman, A.-S., and Omstedt, A.: Measured and simulated latent and sensible heat fluxes at two marine sites in the Baltic Sea, Boundary-Layer Meteorology, 99, 53–84, 2001.

Rutgersson, A., Norman, M., Schneider, B., Pettersson, H., and Sahlée, E.: The annual cycle of carbon dioxide and parameters influencing the air–sea carbon exchange in the Baltic Proper, Journal of Marine Systems, 74, 381–394, https://doi.org/10.1016/j.jmarsys.2008.02.005, 2008.

Rutgersson, A., Norman, M., and Åström, G.: Atmospheric CO_2 variation over the Baltic Sea and the impact on air–sea exchange, Boreal environment research, 14, 238–249, 2009.

Rutgersson, A., Smedman, A., and Sahlée, E.: Oceanic convective mixing and the impact on air–sea gas transfer velocity, Geophysical Research Letters, 38, 2011.

Rutgersson, A., Pettersson, H., Nilsson, E., Bergström, H., Wallin, M. B., Nilsson, E. D., Sahlée, E., Wu, L., and Mårtensson, E. M.: Using land-based stations for air–sea interaction studies, Tellus A: Dynamic Meteorology and Oceanography, 72, 1–23, 2020.

Sahlée, E., Smedman, A. S., Rutgersson, A., and Högström, U.: Spectra of CO_2 and water vapour in the marine atmospheric surface layer, Boundary-layer meteorology, 126, 279–295, 2008.

Schneider, B. and Müller, J. D.: Biogeochemical transformations in the Baltic Sea, Springer, 2018.

Schneider, B., Gülzow, W., Sadkowiak, B., and Rehder, G.: Detecting sinks and sources of CO_2 and CH_4 by ferrybox-based measurements in the Baltic Sea: Three case studies, Journal of Marine Systems, 140, 13–25, 2014.

Sjöblom, A. and Smedman, A.-S.: The turbulent kinetic energy budget in the marine atmospheric surface layer, Journal of Geophysical Research: Oceans, 107, 6–1, 2002.

Smedman, A.-S., Högström, U., Bergström, H., Rutgersson, A., Kahma, K. K., and Pettersson, H.: A case study of air–sea interaction during swell conditions, Journal of Geophysical Research: Oceans, 104, 25 833–25 851, 1999.

Soloviev, A. and Lukas, R.: The near-surface layer of the ocean: structure, dynamics and applications, vol. 48, Springer Science & Business Media, 2013.

Soomere, T.: Numerical simulations of wave climate in the Baltic Sea: a review, Oceanologia, 2022.

Stokes, G. G.: Supplement to a paper on the theory of oscillatory waves, Mathematical and Physical papers, 1, 18, 1880.

Takahashi, T., Sutherland, S. C., Wanninkhof, R., Sweeney, C., Feely, R. A., Chipman, D. W., Hales, B., Friederich, G., Chavez, F., Sabine, C., et al.: Climatological mean and decadal change in surface ocean pCO_2, and net sea–air CO_2 flux over the global oceans, Deep Sea Research Part II: Topical Studies in Oceanography, 56, 554–577, 2009.

Thomas, H. and Schneider, B.: The seasonal cycle of carbon dioxide in Baltic Sea surface waters, Journal of Marine Systems, 22, 53–67, 1999a.

740   Thomas, H. and Schneider, B.: The seasonal cycle of carbon dioxide in Baltic Sea surface waters, Journal of Marine Systems, 22, 53–67, 1999b.

Thomas, H., Pempkowiak, J., Wulff, F., and Nagel, K.: The Baltic Sea, in: Carbon and nutrient fluxes in continental margins, pp. 334–346, Springer, 2010.

Thorpe, S., Osborn, T., Farmer, D., and Vagle, S.: Bubble clouds and Langmuir circulation: Observations and models, Journal of Physical
745   Oceanography, 33, 2013–2031, 2003.

Upstill-Goddard, R. C.: Air–sea gas exchange in the coastal zone, Estuarine, Coastal and Shelf Science, 70, 388–404, 2006.

Van Dam, B. R., Lopes, C. C., Polsenaere, P., Price, R. M., Rutgersson, A., and Fourqurean, J. W.: Water temperature control on CO_2 flux and evaporation over a subtropical seagrass meadow revealed by atmospheric eddy covariance, Limnology and Oceanography, 66, 510–527, 2021.

750   Von Schuckmann, K., Le Traon, P.-Y., Alvarez-Fanjul, E., Axell, L., Balmaseda, M., Breivik, L.-A., Brewin, R. J. W., Bricaud, C., Drevillon, M., Drillet, Y., et al.: The copernicus marine environment monitoring service ocean state report, Journal of Operational Oceanography, 9, s235–s320, 2016.

Wanninkhof, R.: Relationship between wind speed and gas exchange over the ocean revisited, Limnol. Oceanogr.- Meth., 12, 351–362, 2014.

Wanninkhof, R. and McGillis, W. R.: A cubic relationship between air–sea CO_2 exchange and wind speed, Geophysical Research Letters,
755   26, 1889–1892, 1999.

Webb, E. K., Pearman, G. I., and Leuning, R.: Correction of flux measurements for density effects due to heat and water vapour transfer, Quarterly Journal of the Royal Meteorological Society, 106, 85–100, 1980.

Weiss, R.: Carbon dioxide in water and seawater: the solubility of a non-ideal gas, Marine chemistry, 2, 203–215, 1974.

Wesslander, K., Omstedt, A., and Schneider, B.: Inter-annual and seasonal variations in the air–sea CO_2 balance in the central Baltic Sea and
760   the Kattegat, Continental Shelf Research, 30, 1511–1521, 2010.

Woolf, D. K.: Bubbles and the air-sea transfer velocity of gases, Atmosphere-Ocean, 31, 517–540, 1993.

Woolf, D. K.: Bubbles and their role in gas exchange, p. 173–206, Cambridge University Press, 1997.

Woolf, D. K., Shutler, J. D., Goddijn-Murphy, L., Watson, A. J., Chapron, B., Nightingale, P. D., Donlon, C. J., Piskozub, J., Yelland, M. J., Ashton, I., et al.: Key uncertainties in the recent air–sea flux of CO_2, Global Biogeochemical Cycles, 2019.

765   Zhao, D., Toba, Y., Suzuki, Y., and Komori, S.: Effect of wind waves on air–sea gas exchange: Proposal of an overall CO_2 transfer velocity formula as a function of breaking-wave parameter, Tellus B: Chemical and Physical Meteorology, 55, 478–487, 2003.